

LUT UNIVERSITY
LUT School of Energy Systems
LUT Department of Mechanical Engineering

Janne Parviainen

**THE EFFECTS OF LASER WELDING PARAMETERS ON THE WELDABILITY
OF AM IN718 TO WROUGHT 316L STEEL**

14.6.2021

Examiner(s): Professor Heidi Piili, D.Sc. (Tech.)

Junior Research Scientist Saeid Parchegani, M.Sc. (Tech.)

TIIVISTELMÄ

LUT-Yliopisto
LUT School of Energy Systems
LUT Kone

Janne Parviainen

Laserhitsausparametrien vaikutus lisäävällä valmistuksella valmistetun IN718-seoksen ja 316L-teräksen hitsattavuuteen

Diplomityö

2021

71 sivua, 46 kuvaa, 12 taulukkoa ja 3 liitettä

Tarkastajat: Professori Heidi Piili, TkT
Nuorempi tutkija Saeid Parchegani, DI

Hakusanat: Lisäävä valmistus, 3D-tulostus, jauhepetisulatus, laserhitsaus, inconel 718, 316L

Tämän diplomityön tavoitteena on tutkia jauhepetisulatuksella valmistetun IN718 nikkeli-seoksen ja 316L-teräksen laserhitsattavuutta. Tutkimuksessa hyödynnettiin kirjallisuuskatsausta aikaisemmista tutkimuksista sekä kokeellisia testejä.

Teollisuudessa on tarve IN718 ja 316L teräksen hitsaukseen. Tutkimukset jauhepetisulatuksella valmistetun IN718-seoksen ja 316L teräksen hitsattavuudesta ovat kuitenkin harvassa. Aikaisemmista tutkimuksista voitiin kuitenkin todeta, että hitsattavuus on verrattain hyvä ja hitsi saadaan aikaiseksi. Kirjallisuuskatsaus tarkasteli myös jauhepetisulatusta, sillä tuotettujen kappaleiden ominaisuuksia ja kuinka ne vaikuttavat lopputuotteeseen ja sen hitsattavuuteen. Valmistussuunta jauhepetisulatuksessa vaikuttaa valmistettävien kappaleiden kestävyys ja sitä kautta myös hitsin kestävyys.

Kokeellisen osan tarkoituksena oli tutkia IN718:n ja 316L-teräksen välistä hitsiä. IN718 koekappaleet valmistettiin jauhepetisulatuksella niin pysty- kuin vaakasuunnassa. Puolet testikappaleista lämpökäsiteltiin valmistuksen jälkeen. Tällä tavoin valmistussuunnan ja lämpökäsittelyn vaikutusta hitsiin voitiin tutkia tarkemmin. Valmistuksen jälkeen laserhitsaus testit tehtiin LUT-yliopiston Lasertyöstön ja 3D-tulostuksen tutkimusryhmässä.

Hitsien laadun analysointi tehtiin visuaalisella tarkastelulla sekä hitsin poikkileikkauksesta otettujen mikroskooppikuvien avulla. Tuloksista voitiin nähdä, että hitsaus onnistuu ja hyvälaatuinen hitsisauma voidaan saada aikaiseksi. Hitsaus- ja valmistusparametrit vaikuttivat hitsin ulkoiseen laatuun mikä tarkoittaa, että optimaaliset parametrit löydettyäessä hyvälaatuinen hitsi on mahdollinen. Jatkotutkimuksissa valmistussuunnan vaikutusta hitsin laatuun kannattaa tutkia tarkemmin sekä hitsien kestävyttä kokeellisin menetelmin.

ABSTRACT

LUT University
LUT School of Energy Systems
LUT Mechanical Engineering

Janne Parviainen

The effects of laser welding parameters on the weldability of AM IN718 to wrought 316L steel.

Master's thesis

2021

71 pages, 46 figures, 12 tables and 3 appendices

Examiners: Professor Heidi Piili, D.Sc. (Tech.)
Junior Research Scientist Saeid Parchegani, M. Sc. (Tech.)

Keywords: additive manufacturing, powder bed fusion, laser welding, stainless steel, Inconel 718, 316L

The aim of this thesis was to study the laser weldability of laser-based powder bed fusion (L-PBF) manufactured IN718 and wrought 316L steel. This was studied through a literature review of previous studies and experimental testing.

There is a demand in the industrial applications of laser welding of IN718 manufactured by L-PBF to wrought 316L. However, the studies in the literature are limited and there is a knowledge gap to be addressed. It has been however demonstrated that welding of L-PBF parts is possible and a successful weld seam can be produced. Literature review was focused on the characteristics of L-PBF and how it effects the microstructure, mechanical behavior, and weldability of produced parts. The building direction and heat treatment are the important factors that have considerable impact on the characteristics of L-PBF parts, thus, their weldability.

The L-PBF IN718 was manufactured in both vertical and horizontal building directions to further investigate their effect after specimens being welded. Furthermore, half of the AM specimens were heat treated before welding to investigate the effect of heat treatment on the weld quality. Fiber laser welding was carried out with different parameters with the laser processing and additive manufacturing research group at LUT University and weld quality under each parameter was examined.

Welds were analyzed through visual inspection and microscopic images of the weld cross-section. After analyzing all the welds for different qualities and assessing imperfections, the results showed that with the right parameters a good quality weld can be achieved. More studies are however needed to further analyze the strength of the welds with the different welding parameters.

ACKNOWLEDGEMENTS

This thesis was done with the research group of Laser Material Processing and Additive Manufacturing at LUT University. The aim of the thesis was to study the laser weldability of AM IN718 and wrought 316L steel and the effects of different building parameters and laser welding parameters. I would like to thank the research group for this interesting topic and the possibility to do it.

I would like to especially thank Professor Heidi Piili and Junior Research Scientist Saeid Parchegani for their support and guidance throughout this project and for their help whenever it was needed.

Janne Parviainen

Janne Parviainen

Tampere 14.6.2021

TABLE OF CONTENTS

| | |
|--|-----------|
| TIIVISTELMÄ | 1 |
| ABSTRACT | 2 |
| ACKNOWLEDGEMENTS | 3 |
| TABLE OF CONTENTS | 5 |
| LIST OF SYMBOLS AND ABBREVIATIONS | 7 |
| 1 INTRODUCTION | 8 |
| 1.1 Background | 8 |
| 1.2 Aim of the thesis. | 9 |
| LITERATURE REVIEW | 10 |
| 2 INTRODUCTION TO LASER-BASED POWDER BED FUSION | 10 |
| 3 BASIC PROPERTIES OF IN718 | 12 |
| 3.1 Mechanical and chemical properties of IN718 | 12 |
| 3.2 Characteristics of L-PBF produced IN718. | 14 |
| 4 316L STEEL | 17 |
| 5 LASER WELDING OF L-PBF PARTS | 18 |
| 5.1 Laser welding in general | 18 |
| 5.2 Laser welding of L-PBF IN718 parts | 19 |
| 5.3 Experimental set-ups used in laser welding of IN718. | 20 |
| 5.4 Experimental procedures used in laser welding of IN718. | 22 |
| 5.5 Analysis of quality of welds of L-PBF IN718 | 23 |
| EXPERIMENTAL PART | 29 |
| 6 AIM AND PURPOSE OF EXPERIMENTAL PART | 29 |
| 7 EXPERIMENTAL SETUP | 30 |
| 7.1 Welding setup | 30 |
| 7.2 Test specimens | 31 |
| 7.3 Parameters..... | 35 |
| 7.4 Visual inspection method..... | 36 |
| 8 EXPERIMENTAL PROCEDURE | 39 |
| 8.1 Experimental procedure | 39 |
| 8.2 Measuring of weld cross-section | 40 |

| | | |
|-----------|---|-----------|
| 9 | RESULTS AND DISCUSSION | 41 |
| 9.1 | Results of visual inspection. | 41 |
| 9.1.1 | Overall quality | 41 |
| 9.1.2 | Penetration | 44 |
| 9.1.3 | Spatter | 47 |
| 9.1.4 | Root quality..... | 50 |
| 9.1.5 | Heat affected zone. | 53 |
| 9.2 | Results of weld cross-section geometry..... | 56 |
| 9.3 | Imperfections | 60 |
| 9.3.1 | Root concavity | 60 |
| 9.3.2 | Sagging | 62 |
| 10 | CONCLUSIONS..... | 66 |
| 11 | FURTHER STUDIES..... | 68 |
| | LIST OF REFERENCES..... | 69 |

APPENDICES

Appendix I: Parameters for visual inspection

Appendix II: Visual inspection ratings

Appendix II: Figures of welds from experimental testing

LIST OF SYMBOLS AND ABBREVIATIONS

| | |
|---------------|----------------------------------|
| P_{laser} | Laser power [W] |
| Q | Heat input [J/mm] |
| $v_{welding}$ | Welding speed [mm/min] |
| AM | Additive Manufacturing |
| GA | Gas atomization |
| HB | Horizontally built |
| HBHT | Horizontally built, heat treated |
| HAZ | Heat affected zone |
| HIP | Hot isostatic pressing |
| IN | Inconel |
| L-PBF | Laser-based powder bed fusion |
| VB | Vertically built |
| VBHT | Vertically built, heat treated |

1 INTRODUCTION

Additive manufacturing (AM) is a relatively new manufacturing method that has gained a lot of popularity and attention over the recent years. A steady growth of approximately 30 % has been observed annually in the industry and this trend shows no signs of slowing down. There is a growing global demand for digital manufacturing and overall a shift towards more flexibility in manufacturing as AM allows designing parts with virtually no design constraints. AM provides a working solution for this. (Brandt 2017, pp. 2-3; Wits et al. 2015, p. 70; Biffi et al. 2019, p. 1)

1.1 Background

The annual Wohlers report, which provides a worldwide review of AM and 3D-printing annually, gives similar insights for the growth of the industry. It reports that for the past three decades the revenues in the industry have grown annually by an average of 26.7 %. Figure 1 shows the growth in revenue from 1993 to 2019. (Wohlers et al. 2020, pp. 91-93)

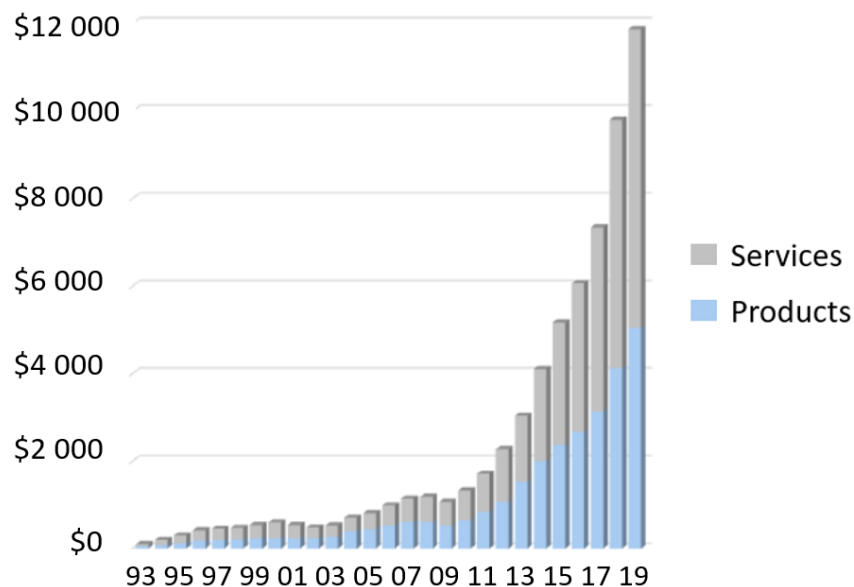


Figure 1. Revenue growth of the AM industry (Modified from Wohlers et al. 2020, p. 93).

Figure 1 depicts the large growth of the industry over the recent years. It shows that both services and products show a large growth over the past years. This all means that AM is an

interesting and important research topic. The growth means higher demand and a need for new and flexible solutions for the growing market.

1.2 Aim of the thesis.

Laser-based powder bed fusion (L-PBF) is the most popular and fastest growing AM technique for manufacturing of metals. L-PBF has many advantages, such as producing highly complex shapes, but one of the largest drawbacks of L-PBF for industrial use is the limitation of the size of the producible parts. The producible part size is limited by the volume of the printing chamber of the AM machines which is usually approximately 300 x 300 x 300 mm. (Brandt 2017, p. 69 ; Yang 2017, p. 63 ; Milewski 2017, pp. 37-38; Wohlers et al 2020, p. 61; Karayel et al. 2020, p. 8 ; Biffi et al. 2019, p. 1 ; Zapf et al. 2020, p. 1)

One solution to solve the size limitation is to join small AM parts to form a large, final part. For metals, this could be done by welding. However, the behavior of AM parts during welding is not yet very well-known which limits applications where a joint is required. (Hawk 2019, p. 3; Yu et al. 2018, p. 20; Mohyla et al. 2020, p. 2) The aim of this thesis is to study the laser beam welding of AM Inconel (IN) 718 superalloy to wrought 316L steel.

Research questions of the thesis are:

- How wrought 316L and AM IN718 can be welded together?
- Which are the optimum welding parameters for joint between 316L and AM IN718?
- What is effect of process parameters on weld joint properties?
- How quality of weld can be evaluated?

Literature review of this thesis will review published, scientific articles on welding of AM parts. The focus is on published articles related to joining of AM parts using laser welding. Welding parameters and microstructural and mechanical properties of welded parts will be categorized based on the different materials. The aim is to find the best range of parameters for welding of AM IN718 and wrought 316L stainless steel and to study the quality of the welds.

LITERATURE REVIEW

2 INTRODUCTION TO LASER-BASED POWDER BED FUSION

L-PBF is the most widely utilized method for metal AM. It is a process in which metal powder is spread and melted layer by layer to form a finished part. The heat source that melts the powder is a laser beam and the process is based on melting the powder in the desired locations. (Diegel et al. 2019, p. 33; Karayel et al. 2020, p. 3; Wits et al. 2015, p. 70)

Figure 2 shows a schematic overview of L-PBF.

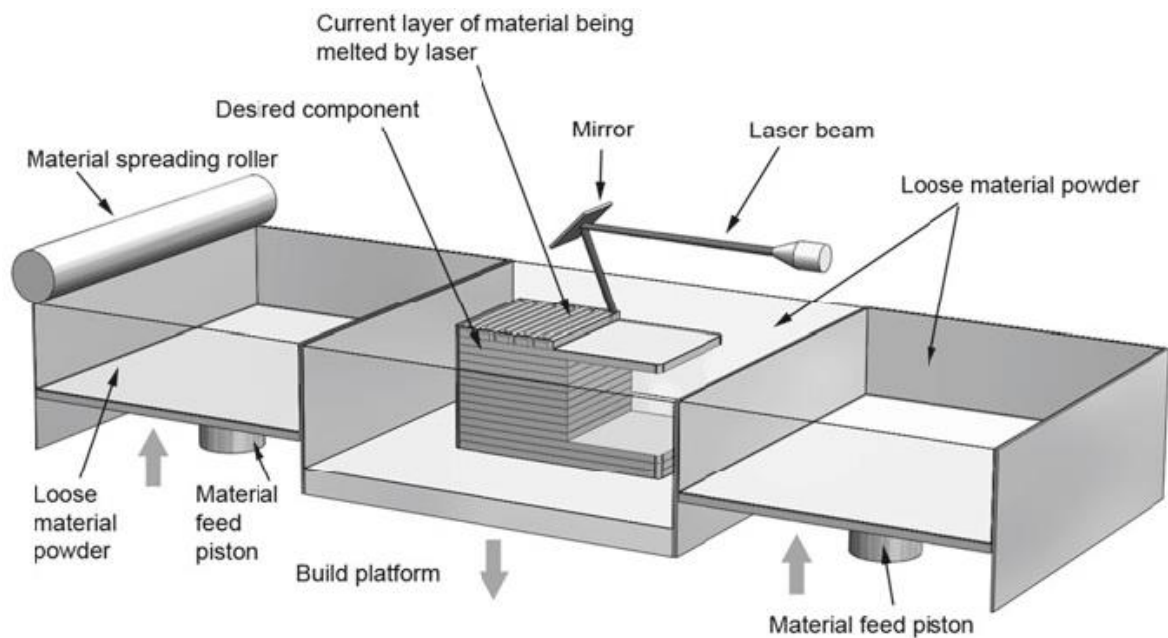


Figure 2. Schematic of L-PBF (Diegel et al. 2019, p. 34).

Figure 2 shows that the L-PBF process works by spreading the material onto the build platform using a recoater. After a thin layer is spread, the laser melts the required powder particles and fuses them together to form the first layer. The build platform is then lowered by a distance equal to the layer thickness and a new layer of powder is laid. Layer thickness is usually between a few tens of microns to approximately 100 microns. This process continues until the part is completely built. After the build is done, which depending on the part size can take several hours, the part is taken out of the building chamber and machined off the building platform. Post-process machining is usually required to reach desired surface quality and shape. (Yang et al. 2017, p. 21)

Parts produced using L-PBF are typically prone to small imperfections and fully dense parts are hard to reach. The layered manner in which the parts are produced leads to non-isotropic behavior where mechanical properties are different depending on the building direction. Surface quality is also usually rougher than parts manufactured with conventional methods which means that post-processing is usually needed to reach the desired surface roughness and quality. (Wits et al. 2015, p. 71; Mohyla et al. 2020, p. 12)

3 BASIC PROPERTIES OF IN718

IN718 is a nickel-based superalloy and one of the most used alloys where high temperature resistance is needed. It is used widely in the aerospace industry in applications such as gas-turbine blades and engines due to its good mechanical properties up to high temperatures of 650°C. (Strößner et al. 2015, p. 1; Prabakaran et al. 2014, p. 1)

IN718 is a good material for AM when welding is needed because it has good weldability compared to other superalloys. (Strößner et al. 2015, p. 1)

3.1 Mechanical and chemical properties of IN718

The chemical composition of IN718 is shown in Table 1.

Table 1. Typical chemical composition of IN718 (Modified from Special Metals 2017, p. 2)

| Element | Weight percentage (%) |
|-------------------------|------------------------------|
| Nickel (plus Cobalt) | 50-55 |
| Chromium | 17-21 |
| Iron | Balance |
| Niobium (plus Tantalum) | 4.75-5.50 |
| Molybdenum | 2.80-3.30 |
| Titanium | 0.65-1.15 |
| Aluminum | 0.20-0.80 |
| Cobalt | Max1.00 |
| Carbon | Max. 0.08 |
| Manganese | Max. 0.35 |
| Silicon | Max. 0.35 |
| Phosphorus | Max. 0.015 |
| Sulfur | Max. 0.015 |
| Boron | Max. 0.006 |
| Copper | Max. 0.30 |

Table 1 presents the chemical composition of IN718. It consists mostly of nickel, chromium, iron, niobium, molybdenum, titanium, and aluminum. The elements of lower quantities are shown in the table.

Table 2 presents the mechanical properties of AM IN718.

Table 2. Mechanical properties of AM IN7180. (EOS 2020, p. 6).

| AM Direction | Yield strength $R_{0.2}$ [MPa] | Tensile strength R_m [MPa] | Elongation at break [%] |
|--------------|-----------------------------------|---------------------------------|----------------------------|
| Vertical | 650 | 970 | 32 |
| Horizontal | 800 | 1090 | 25 |

As Table 2 shows, mechanical properties are different depending on the manufacturing direction. For vertically built specimens, yield strength and tensile strength are lower than horizontally built, but specimens are more ductile. (EOS 2020, p. 6)

Post-build heat-treatments can also be done to IN718 parts to improve strength. Mechanical properties of heat-treated AM IN718 are shown in Table 3.

Table 3. Mechanical properties of heat-treated AM IN718. (EOS 2020, p.6).

| AM Direction | Yield strength $R_{0.2}$ [MPa] | Tensile strength R_m [MPa] | Elongation at break [%] |
|--------------|-----------------------------------|---------------------------------|----------------------------|
| Vertical | 1145 | 1375 | 17 |
| Horizontal | 1240 | 1505 | 12 |

As Table 3 shows, yield strength and tensile strength are higher in heat-treated specimens than without heat treatment. Yield strength of vertically built samples is 495 MPa higher, and tensile strength 405 MPa higher than without heat treatment. For horizontally built specimens the yield strength with heat treatment is 440 MPa and tensile strength 415 MPa higher than without heat treatment. Ductility shows a decrease after heat treatment of approximately 50 %. (EOS 2020, p. 6)

3.2 Characteristics of L-PBF produced IN718.

Parts produced through L-PBF generally have properties comparable to their wrought counterparts. One of the main disadvantages compared to traditionally manufactured parts is that producing completely dense parts is difficult. The combination of printing parameters and their optimization is crucial to achieve as dense parts as possible. Figure 3 shows different printing parameters. (Raza 2020, p. 24)

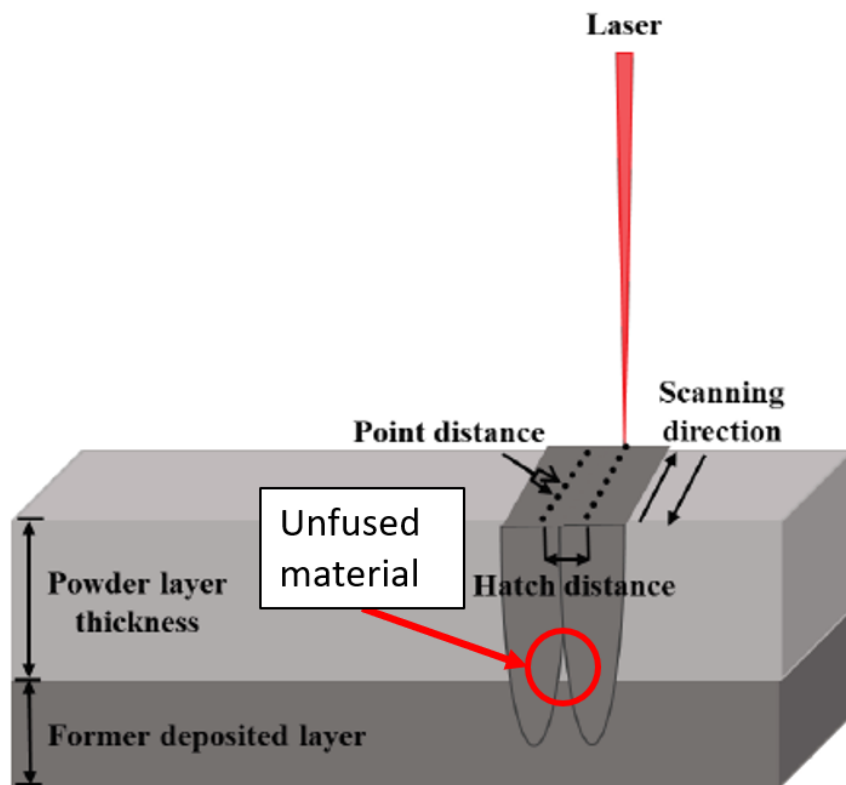


Figure 3. Different printing parameters (Modified from Raza 2020, p. 24).

The shown parameters must all be optimized to avoid unfused material and pores and cavities in the finished part. For instance, if powder layer thickness is too high, the new layer is not fused to the formerly deposited layer if the laser power is not high enough. In case of hatch distance being too much, unfused powder is left between the fusion zones as shown in the figure. These are just a few examples, but overall, unoptimized printing parameters can cause defects in the final part which might influence the weldability of the part. (Raza 2020, p. 24)

The powder can cause problems during the manufacturing process, which can also influence weldability. Gas atomization (GA) is often used to produce the powder for the L-PBF process. Due to the GA process, some common defects can be found in the powder particles. These defects are shown in Figure 4. Particles of the produced powder should not exceed the layer thickness in their size as larger particles will be thrown off the building platform. Overall, GA is often used for powder production because of its lower cost and the particle size distribution is good for L-PBF process. (Raza 2020, p. 21)

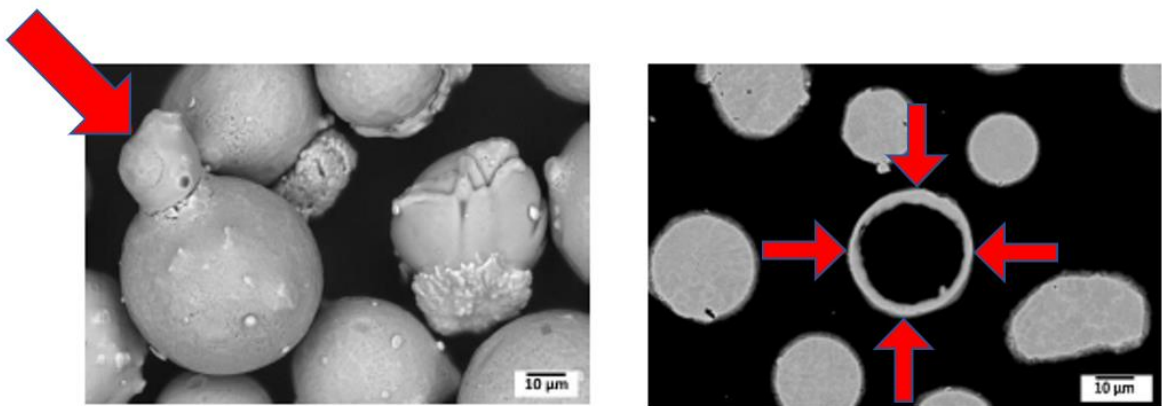


Figure 4. Images showing the satellite particles, and gas entrapped inside powder particle (Modified from Raza 2020, p. 22).

The powder produced using the GA process can contain small amounts of the atomizing gas within the particles and this can lead to porosity for the final products. It is also common for large sized particles produced by GA to have smaller particles attached to them as so-called satellites. These satellites can have a negative effect when the powder is laid (Raza 2020, p. 21)

As the powder is laid on the building platform, it can cause issues with the packing density of the laid powder and issues with spaces left between the powder. These combined with insufficient heat input can cause the powder to not melt properly thus forming unfused or partially fused powder bed. This lack of fusion causes initial cracks inside the material and has a negative effect especially in fatigue strength of the produced part. (Raza 2020, p. 22)

Spherical porosities can be caused by the gas entrapped in the particles, or by trapped shielding gas during the manufacturing process. Small, spherical pores are not so critical for

the strength of the part, but a large number of pores can still have a negative effect on the strength of the final product. If the pores are located on the surface, moisture can get trapped in the and cause the part to be more susceptible to corrosion. (Raza 2020, p. 22)

Strößner et al. (2020, p. 3) conducted a series of tests for L-PBF IN718 test specimens. They found out that the building direction impacts certain material properties which suggests anisotropic behavior. Horizontally built specimens in as-built condition without heat treatment had a higher tensile strength but lower strain until failure when compared to vertically built specimens. Heat treated test samples on the other hand showed significantly higher tensile strength properties than as-built samples. When tensile strength values were compared to wrought IN718 it was found that the tensile strengths were similar, only strain until failure was lower in AM IN718.

Yang et al. (2017, pp. 46-49) reported a series of tests for heat treated L-PBF IN718 tested by Honeywell Aerospace. Three different build orientations were investigated: vertical, horizontal, and 45-degree angle in respect to build plate. These specimens were then subjected to stress relief treatment and hot isostatic pressing (HIP). After the HIP treatment the specimens also went through an additional heat treatment. Specimens were then tested for various material properties and also compared to wrought material. They concluded that the grain size and shape were found to be similar in all specimens, horizontally, vertically and 45-degree built. This would suggest that the microstructure is homogenous in L-PBF IN718 after HIP and heat treatments. They tested the specimens also for tensile strength and found that the results for different build orientations were relatively similar pointing to a uniform texture regardless of build orientation.

4 316L STEEL

316L steel is an austenitic stainless steel. 316L steel has good corrosion resistance and works well in high temperature applications. 316L is the low carbon content variant of 316 steel, hence the letter L. Low carbon content makes 316L steel suitable for welding. (ThoughtCo 2020)

The high temperature resistance means that 316L steel is used in applications such as heat exchangers, valve and pump parts and jet engines. (ThoughtCo 2020)

Table 4 presents the typical chemical composition of 316L stainless steel.

Table 4. Typical chemical composition of 316L stainless steel (Modified from ThoughtCo 2020).

| Element | Weight percentage (%) |
|----------------|------------------------------|
| Carbon | Max. 0.03 |
| Manganese | Max. 2.00 |
| Phosphorus | Max. 0.045 |
| Sulfur | Max.0.03 |
| Silicon | Max. 0.75 |
| Chromium | 16-18 |
| Nickel | 10-14 |
| Molybdenum | 2-3 |
| Nitrogen | Max. 0.10 |
| Iron | Balance |

316L steel consists mostly of chromium, nickel, molybdenum, and iron. Elements of lower content are shown in the table. Carbon content is limited to a maximum of 0.03%.

5 LASER WELDING OF L-PBF PARTS

Laser welding is a process in which laser beam is used as the heat source for a welding process. It is a high-power and high-energy density process for the joining of parts and therefore a very effective joining process.

5.1 Laser welding in general

Laser welding is a joining process where a laser is used to fuse parts together. To briefly describe the process, laser light is fed via mirrors or through an optical fiber from a laser unit to a welding head, and onto the workpiece. The power density of a laser beam is high, which results in a deep and narrow keyhole. (Katayama 2013, p. 3)

Laser welding comes with a number of advantages over conventional welding methods. Low heat input results in a small heat affected zone (HAZ). Low heat input also decreases deformations during welding and welding speed is also usually faster in laser welding compared to conventional welding methods. (Katayama 2013, p. 575) Welding is however a thermal process where the specimens welded will go through a cycle of heating, remelting, and cooling. This process will cause residual stresses in the parts which need to be considered for the end product produced. (Yang et al. 2019, p. 4)

Figure 5 presents a comparison of different welding processes.

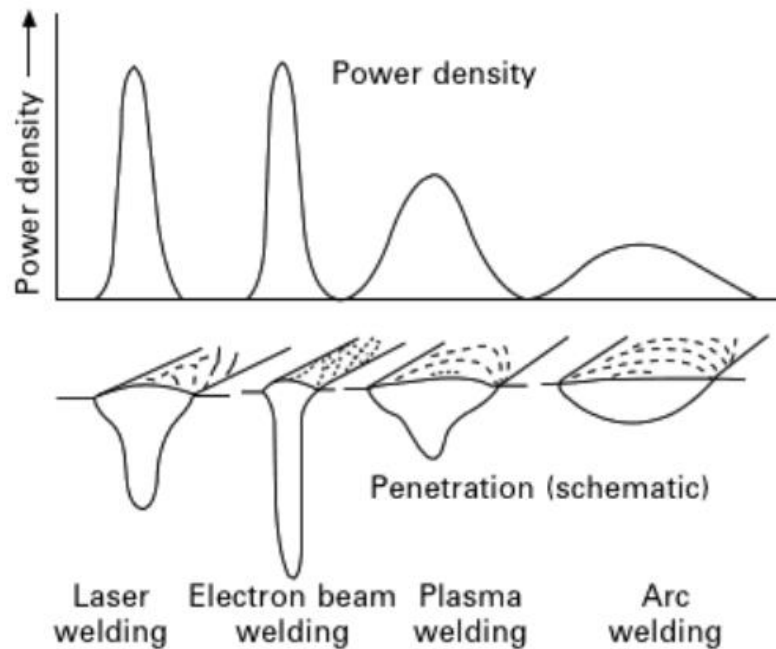


Figure 5. Comparison of different welding processes (Katayama 2013, p. 4).

The figure shows the weld cross-section resulting from different welding methods. When comparing laser welding with traditional arc welding, it can be seen that the power density is high in laser welding and more centralized, whereas in arc welding the density is more spread out through the cross-section. Therefore, laser welding achieves a narrower and deeper weld compared to arc welding. Higher power density of laser welding also means that the heat input is lower which decreases the overall effects of heat in the parts. (Katayama 2013, p. 4)

5.2 Laser welding of L-PBF IN718 parts

Laser welding is becoming the leading welding method for nickel-based alloys due to its advantages over traditional welding methods (Janicki 2015, p. 1). Laser welding of L-PBF IN718 parts has been studied in papers from Hong et al. (2008), Voropaev et al. (2020) and Jokisch et al. (2019). Laser welding of IN718 is used due to the known benefits of laser welding. Laser welding is a process of low heat input and small distortions after welding, rapid welding speed and small HAZ. (Hong et al. 2008)

Possible flaws left from the manufacturing process makes welding of L-PBF parts in general challenging. Parts manufactured using additive manufacturing technologies often have residual porosity in them and are anisotropic. (Voropaev et al. 2020, p. 1)

5.3 Experimental set-ups used in laser welding of IN718.

Voropaev et al. (2020) experimented on welding 2.6 mm, 3.6 mm, 5.1 mm, and 6.1 mm thick L-PBF manufactured IN718 test samples. Test samples dimensions were 100 mm x 50 mm. A 16 kW, LS-16 ytterbium fiber laser with Precitec YW52 laser welding head was used for welding. Focal point was set 10 mm above the top surface. Figure 6 and Figure 7 present



Figure 6. Clamping device used for rigid fixing. (Voropaev et al. 2020, p. 2).

Figure 6 shows the clamping device used and designed by Voropaev et al. (2020) to fix the specimens for welding. The figure shows the base (1), two steel angle plates (2), and tightening screws (3). Figure 7 shows the entire laser welding set-up.

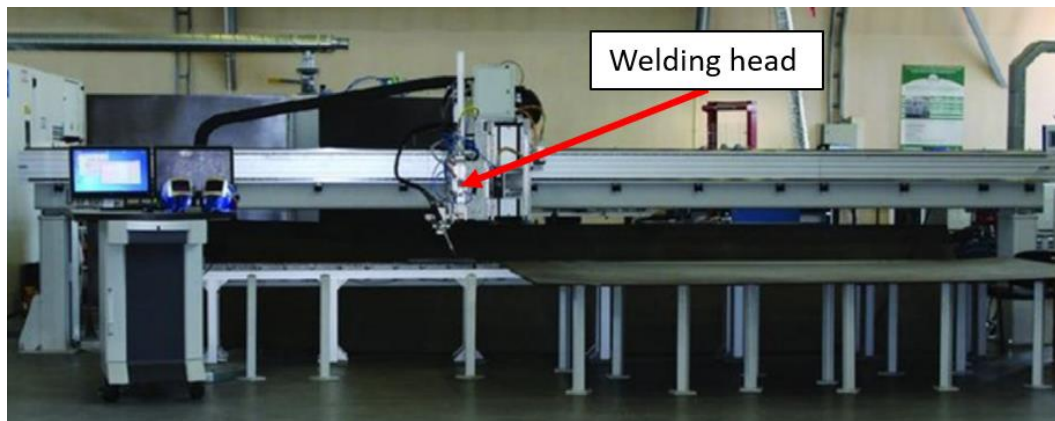


Figure 7. Laser welding set-up. (Voropaev et al. 2020, p. 2).

As Figure 7 shows the laser welding head is mounted on a linear track where the welding is performed.

The microhardness measurements carried out by Voropaev et al. (2020) were done using a Future Tech FM-310 Micro Vickers hardness tester according to the Vickers method at a load of 300 grams. The microscopic images were taken using an optical microscope Leica DMI5000.

Hong et al. (2008) used CO₂ welding to weld wrought IN718 specimens. 5 mm as-rolled specimens were welded using a Trumpf 12000 Turbo continuous wave CO₂ laser with helium as shielding gas. Gas flow was 15 liters/min.

Jokisch et al. (2019) welded L-PBF tubes made of IN718. Tubes were 100 mm in length with diameter of 33 mm and wall thickness of 2.7 mm. 16 kW Yb:YAG disk laser with YW32 laser optic and Precitec scan tracker were used. Optical fiber with core diameter of 200 μm was used to deliver the beam and focal point was set to top surface of the tube. Diameter of the focal point was 420 μm .

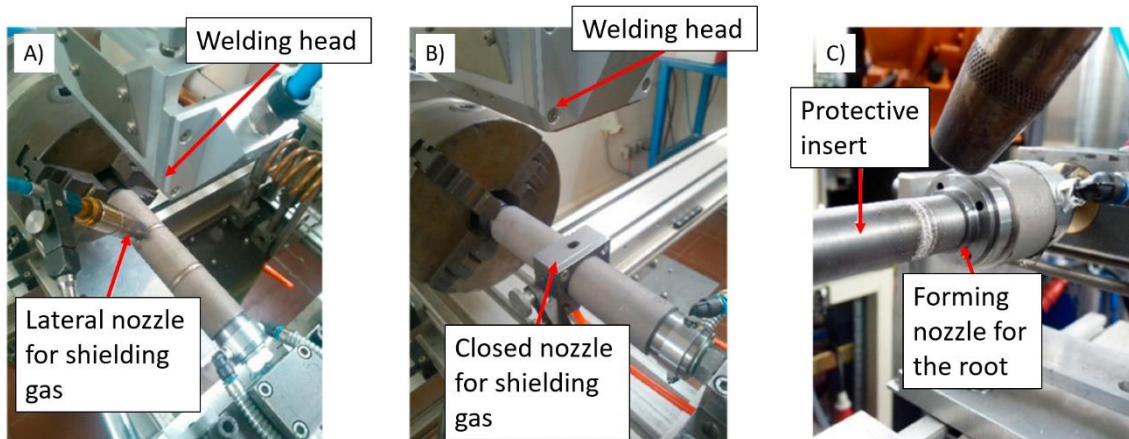


Figure 8. Laser welding setups. (Modified from Jokisch et al. 2020).

As Figure 8 shows the laser welding head is above the welded tubes and remains stationary. The tubes are then rotated to form the weld. Two different set ups for shielding gas were experimented. In A, a lateral nozzle is used for the shielding gas. In B, a closed nozzle is used for shielding gas which distributes shielding gas evenly in the full seam circumference. In C, a protective insert is visible which prevents damages of the insides of the tubes if laser power goes through the tube. A forming nozzle for root gas is used to supply the root forming gas.

Jokisch et al. (2019) measured the residual stresses after welding as well. These measurements were carried out using radiographic residual stress measurements. (Jokisch et al. 2019)

5.4 Experimental procedures used in laser welding of IN718.

Voropaev et al. (2020) Before welding the edges of the samples were cleaned and degreased with acetone. Test specimens were rigidly fixed, and argon inert shielding gas was used during welding.

Hong et al. (2008) welded three types of specimens. As rolled, 955°C solution treatment and 955°C solution treatment and aging. Different types of heat treatments were also done after welding: as welded, direct aging, 955°C solution treatment and aging, and cyclic solution heat treatment. The cyclic solution heat treatment was done by holding the specimen at 1000°C for 3 minutes, then cooling at a rate of 3°C/min and then holding at 985°C for 8 minutes. This treatment was done three times in a row.

In the experiments carried out by Jokisch et al. (2019), half of the test specimens were heat treated before welding and edge quality varied between machined and as built. Laser power was varied between 1.6 kW and 2.4 kW and welding speed varied between 1 m/min and 1.5 m/min.

Residual stress measurements were done as presented in Figure 9.

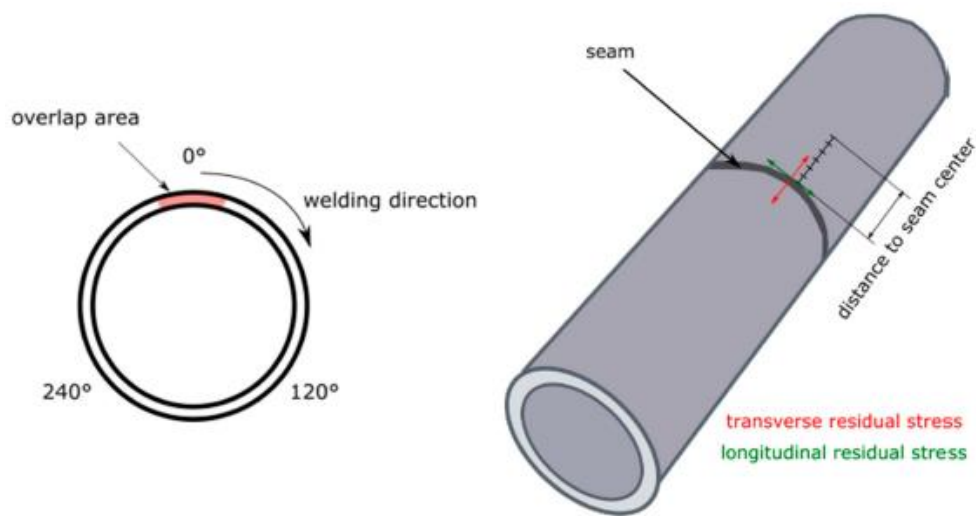


Figure 9. Residual stress measurements. (Jokisch et al. 2019).

Residual stresses were first measured in 30 points on a calibration sample. This results from 5 measuring points in two measuring directions and 3 points on the weld seam. The three points on the seam were separated by 120°. After evaluating the results in these 30 points, the points of highest residual stresses were located, and the future samples were measured in these locations only. (Jokisch et al. 2019, p. 4)

5.5 Analysis of quality of welds of L-PBF IN718

Voropaev et al. (2020) achieved full penetration welds with all combinations of parameters. Table 5 shows the welding parameters used by Voropaev et al. (2020).

Table 5. Welding parameters (Modified from Voropaev et al. 2020, p.3).

| Specimen | Plate thickness (mm) | Laser power (kW) | Welding speed (m/min) |
|----------|----------------------|------------------|-----------------------|
| A | 2.6 | 2.5 | 3.6 |
| B | 3.6 | 3.5 | 2.4 |
| C | 5.1 | 3.5 | 1.5 |
| D | 6.2 | 3.5 | 0.6 |

As Table 5 shows, welding power and welding speed were altered for four different thicknesses: 2.6 mm, 3.6 mm, 5.1 mm and 6.2 mm. For 2.6 mm plate thickness laser power was 2.5 kW, for thicknesses 3.6 mm, 5.1 mm and 6.2 mm the laser power was a constant 3.5 kW. Welding speed Figure 10 presents microsections of welds A, B, C and D from Voropaev et al (2020).

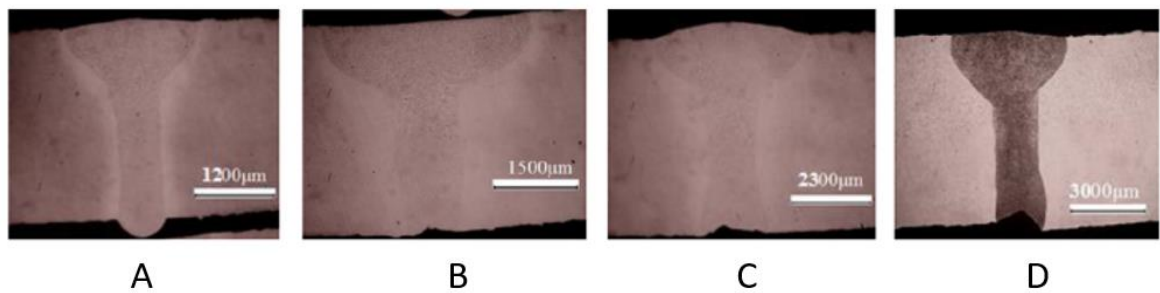


Figure 10. Weld microsections with different welding parameters (Modified from Voropaev et al. 2020).

Figure 10 shows is that all parameters result in full penetration welds. Shape of the weld beads are slightly different depending on the parameters used for laser welding. Weld A is 2.6 mm plate. Weld is fully penetrated but excess weld can be seen on the root side. Weld B is to 3.6 mm plate, and it is more T-shaped with a wide top and narrow root. Slight concavity can be seen on the root side. Weld C is to 5.1 mm plate. Excess weld metal can be seen on the top and root concavity on the root side. The narrowest weld D is found in the largest plate thickness of 6.2 mm. Top side of the weld is good cavity however root concavity is visible on the root side of the weld.

Microhardness tests were carried out as well. Lowest microhardness values were found in specimen D, 253 HV, and highest microhardness in specimen A, 379 HV. This might be due

to different temperature gradients and the cooling rate of the metal during the L-PBF process. Microhardness of the samples was also measured after post-weld heat treatment and the weld seam photographed. Results can be seen in the following figures. (Voropaev et al. 2020, p. 3-4)

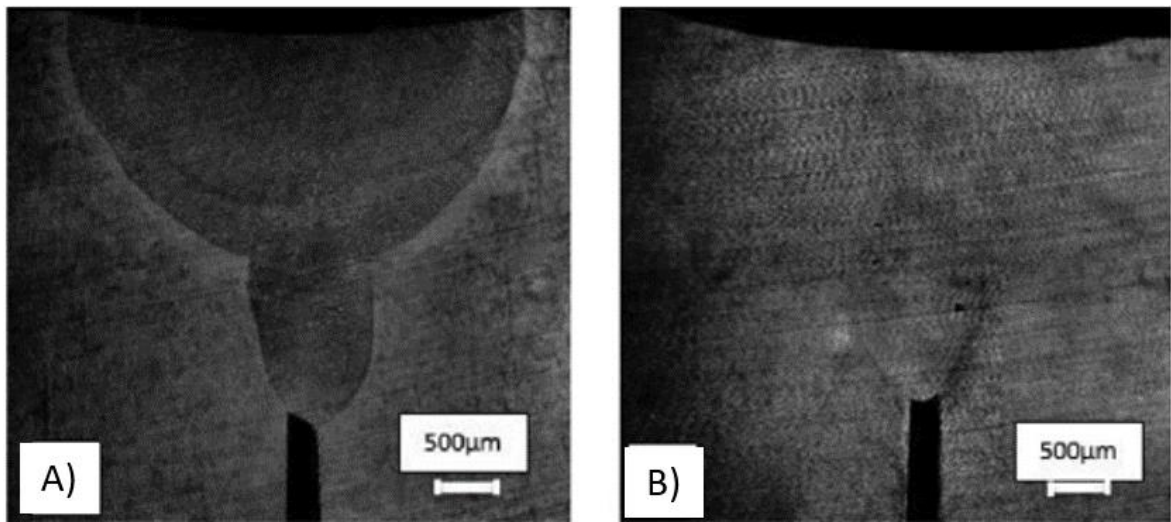


Figure 11. Results before heat treatment and after heat treatment (Modified from Voropaev et al. 2020, p. 4).

As Figure 11 shows, it was found that after the post-weld heat treatment, the base material and weld seam become homogenous. Figure 8a shows the cross-section before heat treatment, and figure 8b shows the cross-section after heat treatment. The visible border between the base material and the weld material is almost completely removed with post-weld heat-treatment. Figure 12 presents the results of microhardness tests.

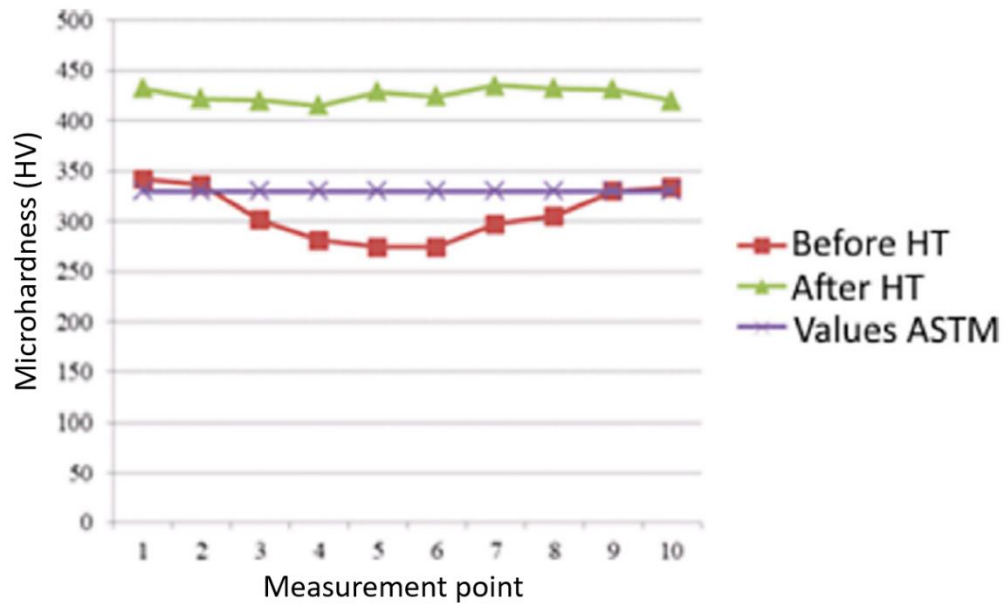


Figure 12. Microhardness results (Modified from Voropaev et al. 2020, p. 4).

As Figure 12 shows, the local decrease in microhardness in the area of the weld seam is removed by using post-weld heat-treatment which results in equal microhardness throughout the cross section. It was also determined that rigidly fixing the welded parts reduced the deformations caused by welding by 30 %. Microhardness is also observed to increase in laser welded IN718, with marginal decrease as welding speed is decreased. (Voropaev et al. 2020, p. 3-5; Sharma et al. 2020, p. 18)

Hong et al. (2008) discovered that the optimum parameters for a full penetration butt weld with CO₂ laser on 5 mm IN718 plates are presented in Table 6.

Table 6. Optimal parameters according to Hong et al. (2008) p. 5.

| Laser power (kW) | Welding speed (m/min) |
|------------------|-----------------------|
| 6.0 | 2.5 |
| 8.0 | 4.0 |

As seen in the table, two parameter sets were found to be adequate. In both sets the focus position is at top surface of plate. When moving the focal position 2 mm above the surface, porosities were observed, and the welds were only partially penetrated. When focal position

was 2 to 3 mm below top surface, spatters were found, and the welds were concave. (Hong et al. 2008, p. 3)

Varying the welding speed had similar results. At 6 kW laser power, lowering the welding speed down to 1.5 m/min resulted in cracks and spatters. When increasing speed to 3.0 m/min and above, full penetration weld could not be achieved anymore. Spatters and cracks were observed also at 8 kW laser power when welding speed was below 3.5 m/min and at laser power of 10 kW. It was therefore concluded that the parameters shown in Table 6 are optimal. (Hong et al. 2008, p. 3)

Hong et al. (2008, p. 5) tested the tensile strength properties of welded specimens. Specimens had different treatments: as-rolled, pre-heat treated, post-weld heat treated and different combinations of these. Tensile strength was found to be similar in as rolled and post-weld heat treated samples, varying between 1206 MPa and 1380 MPa. However, in samples that were not post-weld heat treated, the tensile strength was 989 MPa. This suggests that post-weld heat treatment influences tensile strength properties of welded IN718.

Jokisch et al. (2019) experimented on welding tubes made of L-PBF IN718. They found a difference in the weld seam quality depending on whether the edge was machined or not. This is shown in Figure 13.

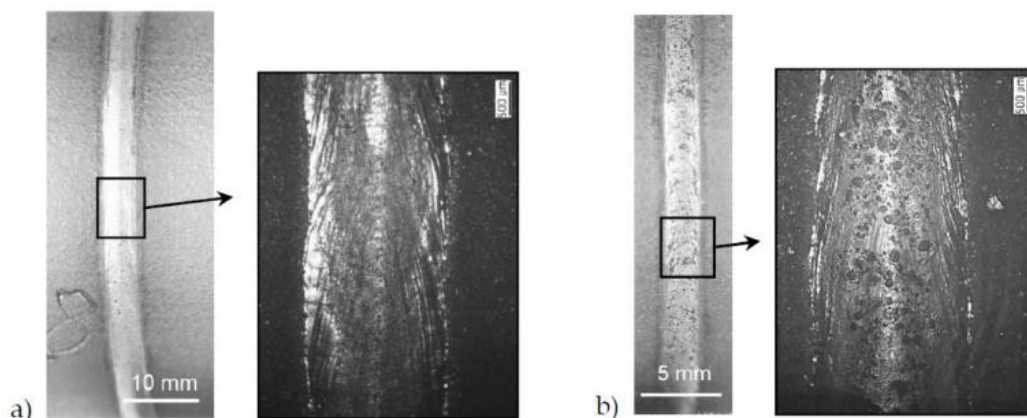


Figure 13. Appearance of weld seam, a) machine cut edge, b) as-built edge. (Jokisch et al. 2019, p. 6).

As it can be seen from figure 13, the machined edge shows a shiny surface, whereas the as-built edge shows inclusions on the seam and they could exist inside the weld metal as well, which is not desired. These inclusions are not present in machine cut edge. It is supposed that these inclusions on the as-built edge are caused by the AM process which leaves a rough surface. During the welding, the inclusions floated towards the weld pool surface. Because the machined edge is smooth before welding already, there are no inclusions to float to the surface, and the end result is a shiny surface. (Jokisch et al. 2019, p. 13)

Residual stresses were also investigated by Jokisch et al. (2019). It was found that heat treated parts had lower residual stresses after welding than as-built samples. As built specimens had residual stresses of 400 MPa and heat-treated specimens had residual stresses of 30 MPa. (Jokisch et al. 2019, p. 7)

EXPERIMENTAL PART

Experimental testing was conducted as part of the thesis. In the testing, test specimens of AM IN718 were laser welded to 316L steel using different laser welding parameters. After welding, the seams were visually observed for the quality of the seam, and microscopically observed for the quality of the microstructure. This way the effect of different welding parameters on the quality of the weld seam could be studied.

6 AIM AND PURPOSE OF EXPERIMENTAL PART

The experimental tests were set up to study the dissimilar joint between AM IN718 and 316L steel in more detail. Previous studies have been conducted as introduced in the literature review, but more information is still needed in this area.

The specimens of wrought 316L steel are all similar. However, L-PBF IN718 are manufactured in a few different ways. Specimens are manufactured with horizontal and vertical position and a portion of these are also heat treated. The parameters of the L-PBF process are the same for all specimens.

In the welding tests, welding speed and laser power are varied. The aim is to find out how changing these parameters affect the weld quality and microstructure of the weld.

7 EXPERIMENTAL SETUP

Testing setup is presented in this chapter. Testing setup consists of laser, welding robot, welding head, shielding gas, and clamping of test specimens.

7.1 Welding setup

The experimental tests were carried out in the laser processing laboratories at LUT University in Lappeenranta, Finland. In the tests, additively manufactured specimens of IN718 alloy were laser welded to wrought 316L steel. Figure 14 presents the welding setup.

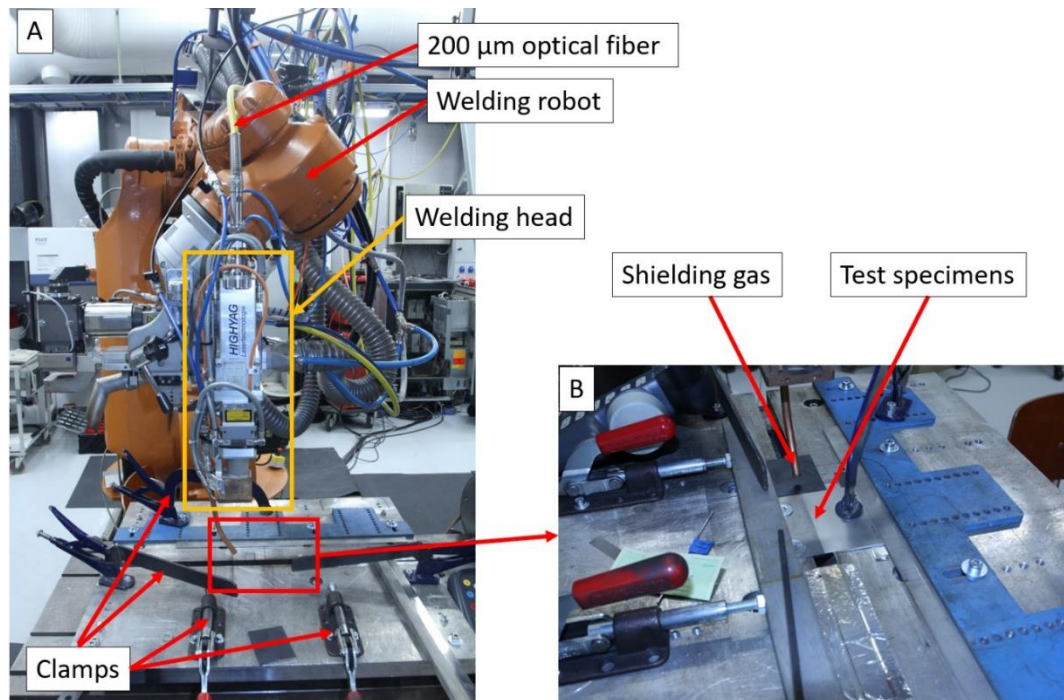


Figure 14. Laser-welding setup for experimental testing.

Figure 14A shows a general overview of the setup. The KUKA KR125 robot holds the Highyag laser processing head BIMO circled in yellow. A 200 µm optical fiber was used to deliver the laser beam from the laser unit to the welding head. The laser unit was a 10 kW IPG YLS-10000-S4.

Figure 14B is a close-up of the squared area. It shows the test specimens in the center and the way they were rigidly fixed to the table. The shielding gas dispenser is also shown. Argon was used as the shielding gas. The specimens of IN718 and 316L steel were carefully placed in a way that the laser beam is as close to center of the seam as possible. Then clamps were used to fix the specimens rigidly in place. Under the shielding gas tube can be seen a darker plate which was used as starting point for weld. This way the robot had time to accelerate to wanted welding speed before hitting the test specimens.

Figure 15 presents the welding head.

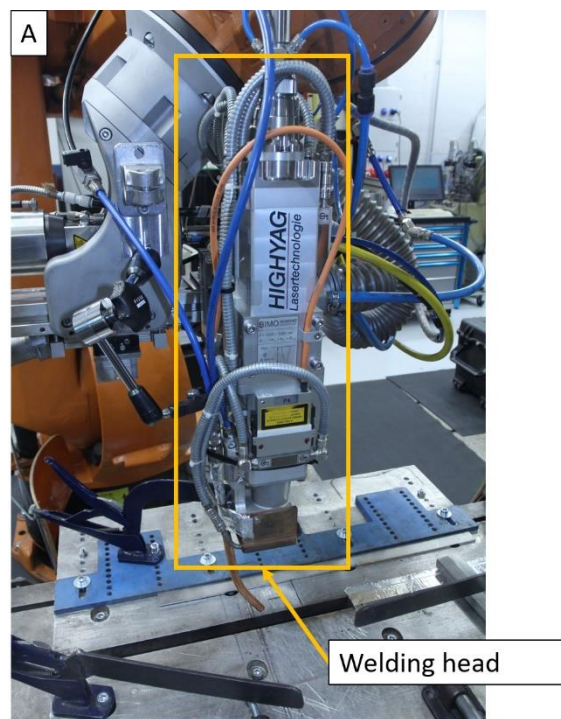


Figure 15. Welding head including collimation and focusing.

Figure 15 shows the Highyag welding head. The collimation and focusing modules used and the 200 μm optical fiber result in a 420 μm diameter focal point. (Highyag 2012, p. 19)

7.2 Test specimens

Test specimens for the experiments were wrought 316L steel and L-PBF IN718. IN718 parts were produced by Delva Oy using proprietary printing parameters. Dimensions of test specimens are shown in Figure 16.

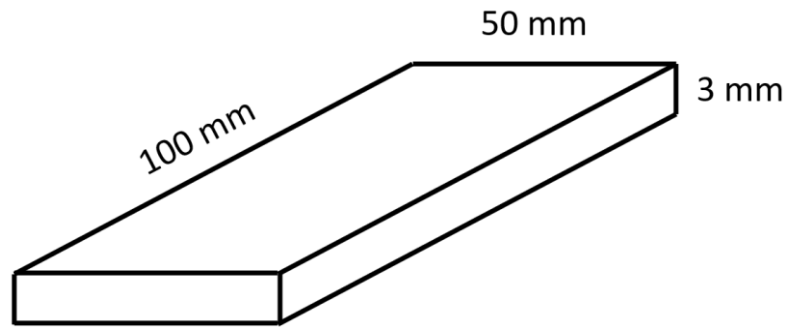


Figure 16. Test specimen dimensions.

As figure 16 shows the test specimens were 100 mm x 50 mm x 3 mm. Welding was done along the long, 100 mm side.

For the IN718 specimens, two different manufacturing positions were used: horizontal and vertical. This and the locations on the L-PBF platform are demonstrated in Figure 17.

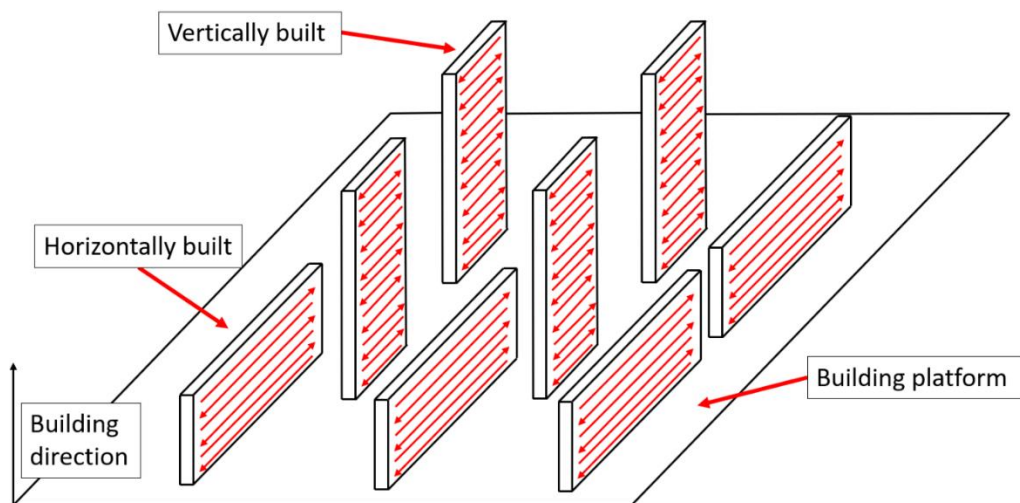


Figure 17. Manufacturing of the IN718 specimens.

A total of 18 vertically built and 18 horizontally built specimens were manufactured. Figure 17 shows the L-PBF building platform and how the specimens were placed and manufactured. The arrows inside the specimens show how the layer-by-layer building was performed. Half of specimens from both building directions were also heat treated after printing. This adds up to a total of 36 test specimens. Table 7 summarizes the IN718 specimens.

Table 7. Summary of IN718 test specimens.

| # of specimens | Vertically built (VB) | Horizontally built (HB) | Vertically built, heat treated (VBHT) | Horizontally built, heat treated (HBHT) |
|----------------|-----------------------|-------------------------|---------------------------------------|---|
| 9 specimens | X | | | |
| 9 specimens | | X | | |
| 9 specimens | | | X | |
| 9 specimens | | | | X |

Abbreviations for test specimens shown in Table 7 are used for the rest of the thesis. The edges of the AM IN718 parts were machined for better edge quality. Machining the welded edge smooth helps to form a good weld seam and makes the tests more repeatable. Figure 18 shows the test specimens.



Figure 18. Test specimens.

As Figure 18 shows, the heat treated IN718 test specimens are dark colored. To help with the laser absorption during welding, the dark color was grinded off the specimens. This process is seen in Figure 19.

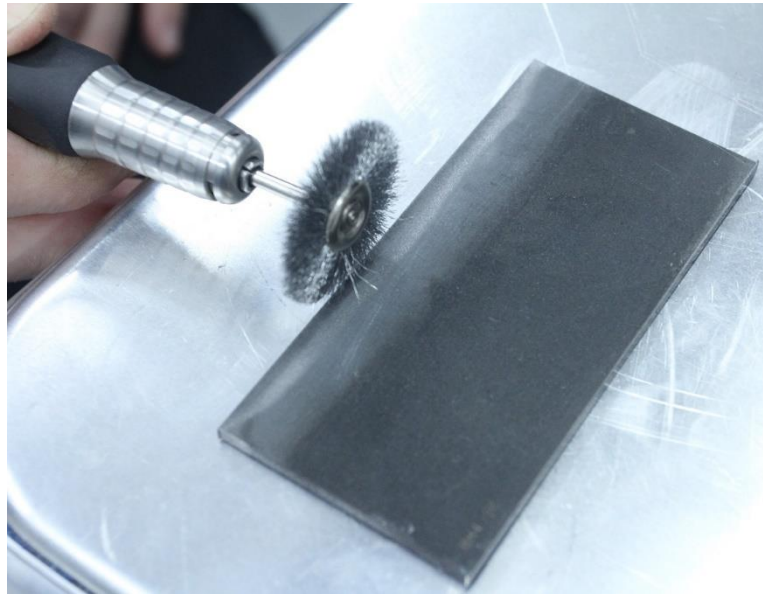


Figure 19. Grinding of edge.

As figure 19 shows the heat-treated plates of IN718 were ground with a steel brush to make the surface clearer and better for welding. Then as the specimens were placed on the table for welding. Figure 20 presents how the specimens were place for welding.

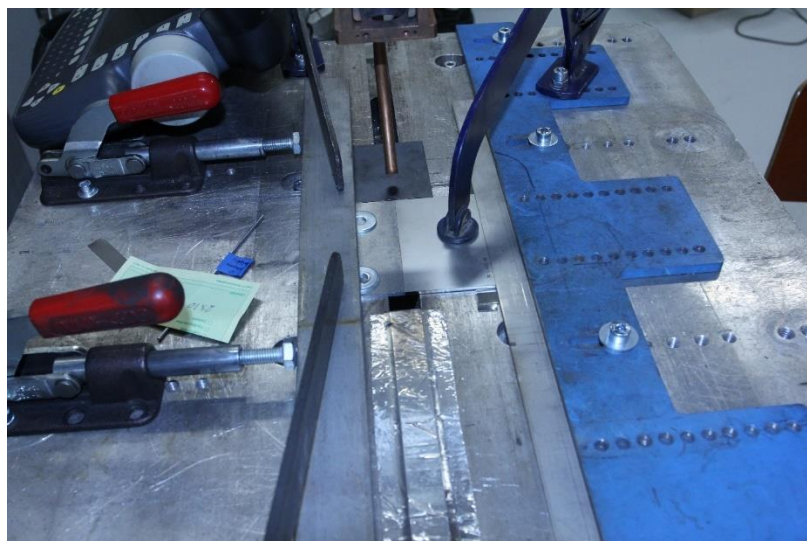


Figure 20. Specimens placed for welding.

As figure 20 shows, the specimens were fixed using clamps to ensure they are rigidly fixed to the table. After fixing the specimens the laser power was set to the laser and welding speed was set to the robot and the welding was performed with a continuous flow of shielding gas.

7.3 Parameters

L-PFB manufacturing process was conducted by Delva Oy and therefore the parameters for the process are not public. However, some general information about L-PBF IN718 can be found in EOS material datasheet for AM IN718. (EOS 2020, p.3)

The heat treatment before welding was done according to aerospace material specifications AMS 2774 and AMS 5662. Heat treating the specimens after L-PBF process relieves residual stresses formed during manufacturing and a microstructure of gamma double prime precipitates is formed. The heat treatment consists of two steps:

- Step I. Solution annealing. Holding at 954 °C for one hour per 25 mm of thickness. Air or argon cooling afterwards.
- Step II. Ageing treatment. Holding at 718 °C for 8 hours, furnace cooling to 621 °C and holding at 621 °C for a total of 18 hours. Air or argon cooling afterwards. (EOS 2020, p. 4)

Welding was done using nine different parameter sets. In these sets the shielding gas, beam spot and focal position were kept constant throughout, and welding speed and laser power were changed. Each specimen described in Table 7 was welded with the following nine different parameter sets presented in Table 8. The equation to obtain heat input is shown in equation 1.

$$Q = \frac{P_{laser}}{v_{welding}} \quad (1)$$

, where Q is heat input [J/mm], P_{laser} is laser power (W) and $v_{welding}$ is welding speed [mm/min].

Table 8. Welding parameter sets.

| Parameter set | Laser power (kW) | Welding speed (m/min) | Heat input (J/mm) | Beam spot (mm) | Focal position |
|---------------|------------------|-----------------------|-------------------|----------------|----------------|
| 1 | 2.5 | 1.0 | 150 | 0.5 | -2 |
| 2 | 2.5 | 1.5 | 100 | 0.5 | -2 |
| 3 | 2.5 | 2.0 | 75 | 0.5 | -2 |
| 4 | 3.0 | 1.5 | 120 | 0.5 | -2 |
| 5 | 3.0 | 2.0 | 90 | 0.5 | -2 |
| 6 | 3.0 | 2.5 | 72 | 0.5 | -2 |
| 7 | 3.5 | 2.0 | 105 | 0.5 | -2 |
| 8 | 3.5 | 2.5 | 84 | 0.5 | -2 |
| 9 | 3.5 | 3.0 | 70 | 0.5 | -2 |

As can be seen from table 8, laser power is increased gradually from 2.5 kW to 3.5 kW and welding speed varies between 1.0 m/min to 3.0 m/min. With these parameters the heat input is between 70 J/mm and 150 J/min.

7.4 Visual inspection method

The results of the experimental tests consist of visual inspection of the weld seam and the area of the weld in general as well as microstructural study of the weld cross-section. Visual inspection is done by using a scale from 1 – very bad to 5 – very good and different categories are judged using this scale.

The welds were judged based on 5 categories. Overall quality, penetration, spatter, root quality and size of the heat affected zone. For overall quality, all the other categories were considered when judging the best and worst specimens. For penetration it was assessed whether the weld was fully penetrated or not and, and if fully penetrated, how well the weld is fully penetrated. Spatter was assessed by viewing both sides of the weld and evaluating the amount of spatter in the vicinity of the weld. For good root quality, the root should be as smooth and spatter free as possible. Heat affected zone should be as small as possible while still achieving a good, full penetration weld.

Table 9 presents the visual inspection scales with example figures for each category.

Table 9. Visual inspection scales.


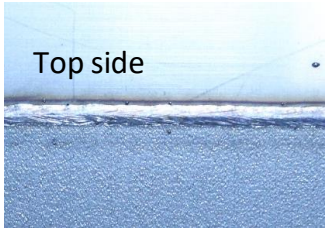
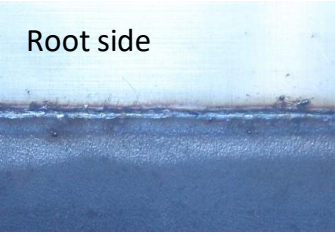
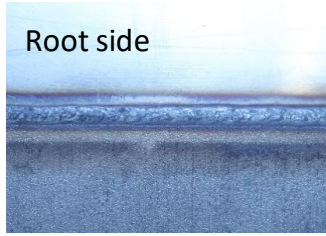
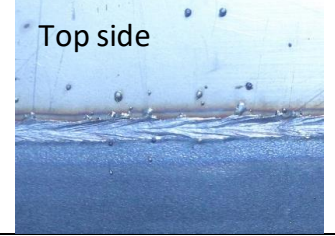
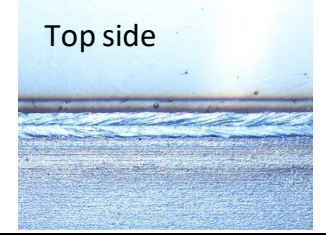
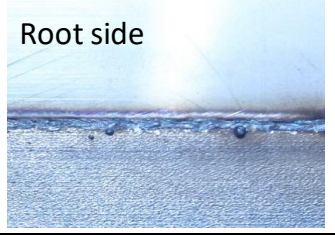
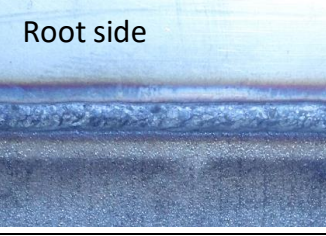
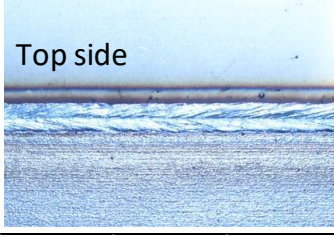
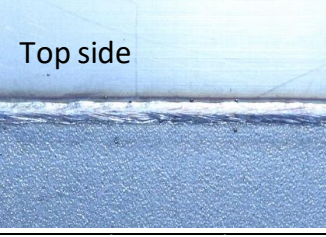
| Overall quality | | | | |
|--|---|---|---|---|
| Very bad | | | | Very good |
| 1 | 2 | 3 | 4 | 5 |
| Top side  | | | | Top side  |
| Penetration | | | | |
| Very bad | | | | Very good |
| 1 | 2 | 3 | 4 | 5 |
| Root side  | | | | Root side  |
| Spatter | | | | |
| Very bad | | | | Very good |
| 1 | 2 | 3 | 4 | 5 |
| Top side  | | | | Top side  |
| Root quality | | | | |
| Very bad | | | | Very good |
| 1 | 2 | 3 | 4 | 5 |
| Root side  | | | | Root side  |
| Heat affected zone (HAZ) | | | | |
| Very bad | | | | Very good |
| 1 | 2 | 3 | 4 | 5 |
| Top side  | | | | Top side  |

Table 9 first presents the difference in overall quality of the weld. In the weld where overall quality has been rated as 1, a lot of spatter can be seen on the top side of the weld, whereas there is no visible spatter in the weld rated as 5. For overall quality, the root side is also examined and considered. In penetration, the larger the weld pool is on the root side, the better the penetration of the weld. For a good weld, the weld should be fully penetrated.

Spatter is rated by examining the top side of the weld and assessing the amount of spatter. For a very good weld, there should be no visible spatter. As the example for a very bad weld shows, a lot of spatter can easily be seen. For the root quality to be very good, the weld can be seen to be smooth and even. If the root quality is assessed as very bad, bubbles and spatter can be seen on the root side and the weld is not smooth. For a very good HAZ, the HAZ should be as small as possible and vice versa for a very bad HAZ. The parameters for the welds in Table 9 are found in appendix I.

8 EXPERIMENTAL PROCEDURE

Experimental testing was conducted to study the weldability of IN718 and 316L. This chapter will present the experimental procedure as well as the parameters used in the L-PBF process, heat treatment and welding tests.

8.1 Experimental procedure

The experiments began by laser marking the IN718 specimens according to their manufacturing position, vertical or horizontal, and whether they had been heat treated or not. An example of this is shown in Figure 21.

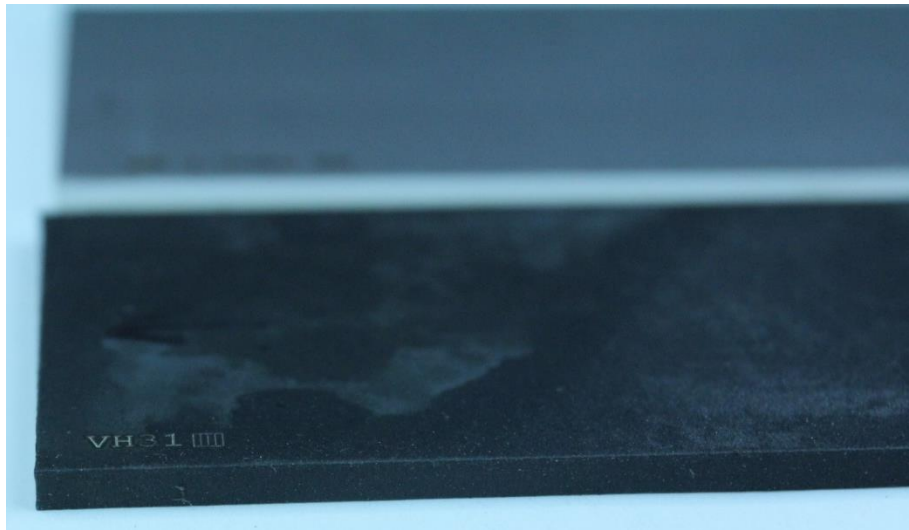


Figure 21. Example of laser marking of IN718 specimens.

The specimens were laser marked in the corners as shown. This way it was clear which specimens were which after the welding.

After marking the specimens, the welding was done. The specimens were placed on the table and clamped as similarly each time as possible. Results were documented and photographed carefully after welding. Documented results are found in appendix I.

8.2 Measuring of weld cross-section

The welded test specimens were sawed in the middle and the cross-section surface polished to be able to analyze the weld geometry. The welds were measured from the top, the middle, and the bottom for their width and results documented. Figure 22 presents the locations for the measurements.

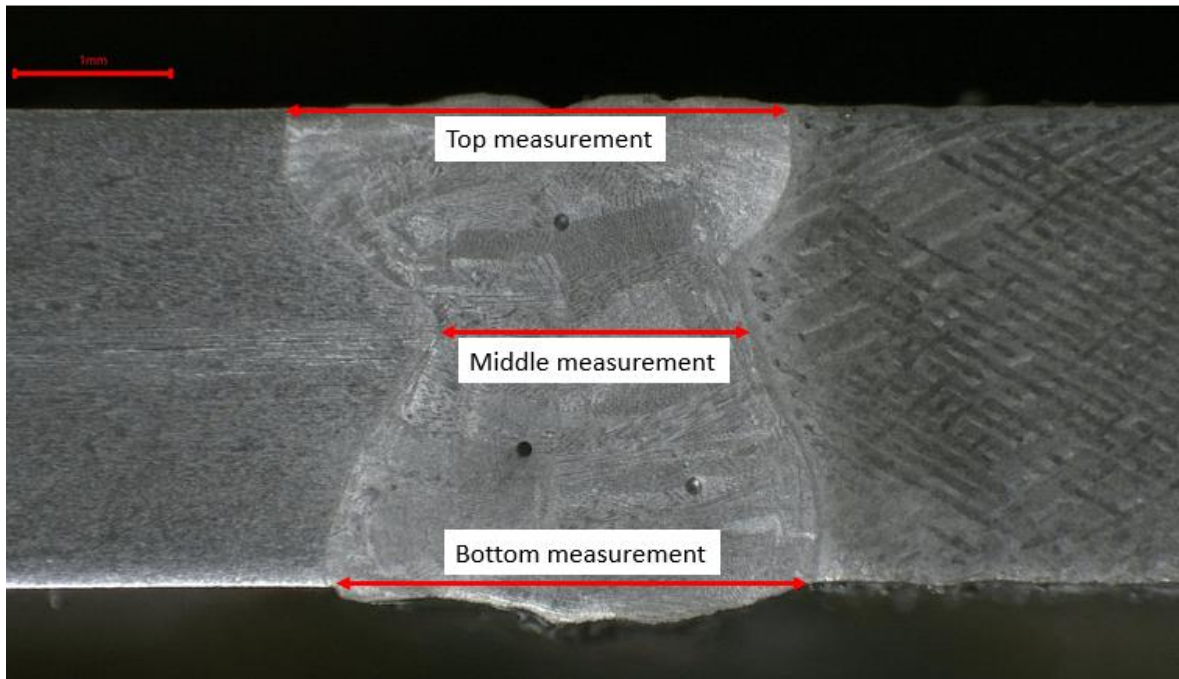


Figure 22. Width measurement locations.

As Figure 22 shows, the measurements were done from the top surface, from the thinnest part in the middle and from the bottom surface.

9 RESULTS AND DISCUSSION

The following sections will present the results of the welding experiments. Results of visual inspection and microstructural analysis will be shown in figures. Appendix III presents the pictures taken of all the welds for the experimental part.

9.1 Results of visual inspection.

Visual inspection began by finding all the welds that meet the criteria of very bad and very good for the different results as presented in the previous sections. This way the good and bad parameters can be found. Appendix II presents the tables used for drawing the graphs.

9.1.1 Overall quality

Overall quality was judged based on the criteria presented in Table 9. It is calculated as an average of the other categories, meaning that in order to be rated good in overall quality, the weld must be high quality in all other categories as well.

The following figures present the overall quality results. The graphs are separated by the welding power.

Figure 23 presents the overall quality with 2.5 kW welding power.

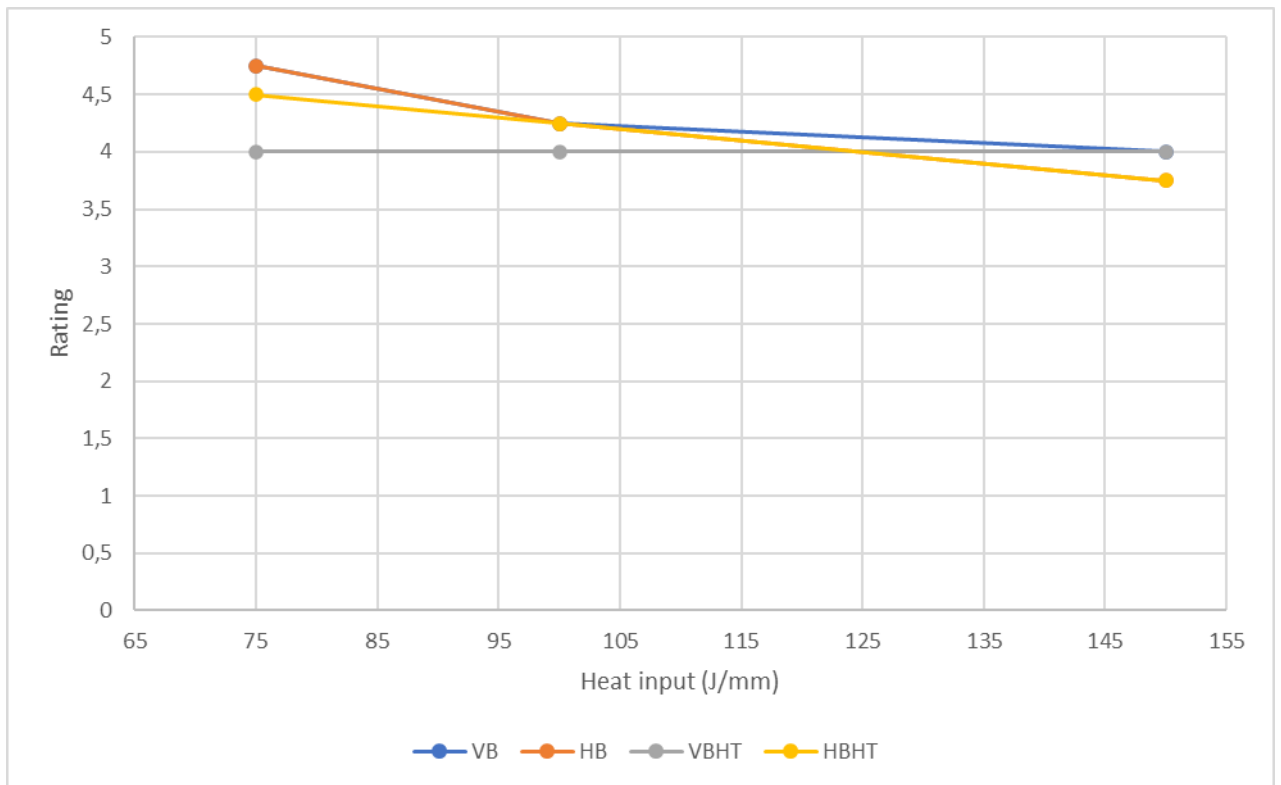


Figure 23. Overall quality, 2.5 kW welding power, welding speed 1.0 m/min, 1.5 m/min and 2.0 m/min.

Figure 23 presents how overall quality of the weld changes with 2.5 kW constant welding power and gradually decreasing the welding speed, which results in an increase in heat input. What can be seen is that the overall quality is decreased with increase in heat input, although not drastically. The non-heat-treated specimens appear to have the best overall quality compared to the heat-treated specimens. Although sample size is small, this indicates that at 2.5 kW laser power, a higher speed and therefore a lower heat input results in a better-quality weld. The highest quality appears to be with the vertically manufactured specimens with highest rating being at 4.75.

Figure 24 presents overall quality for constant laser power of 3.0 kW.

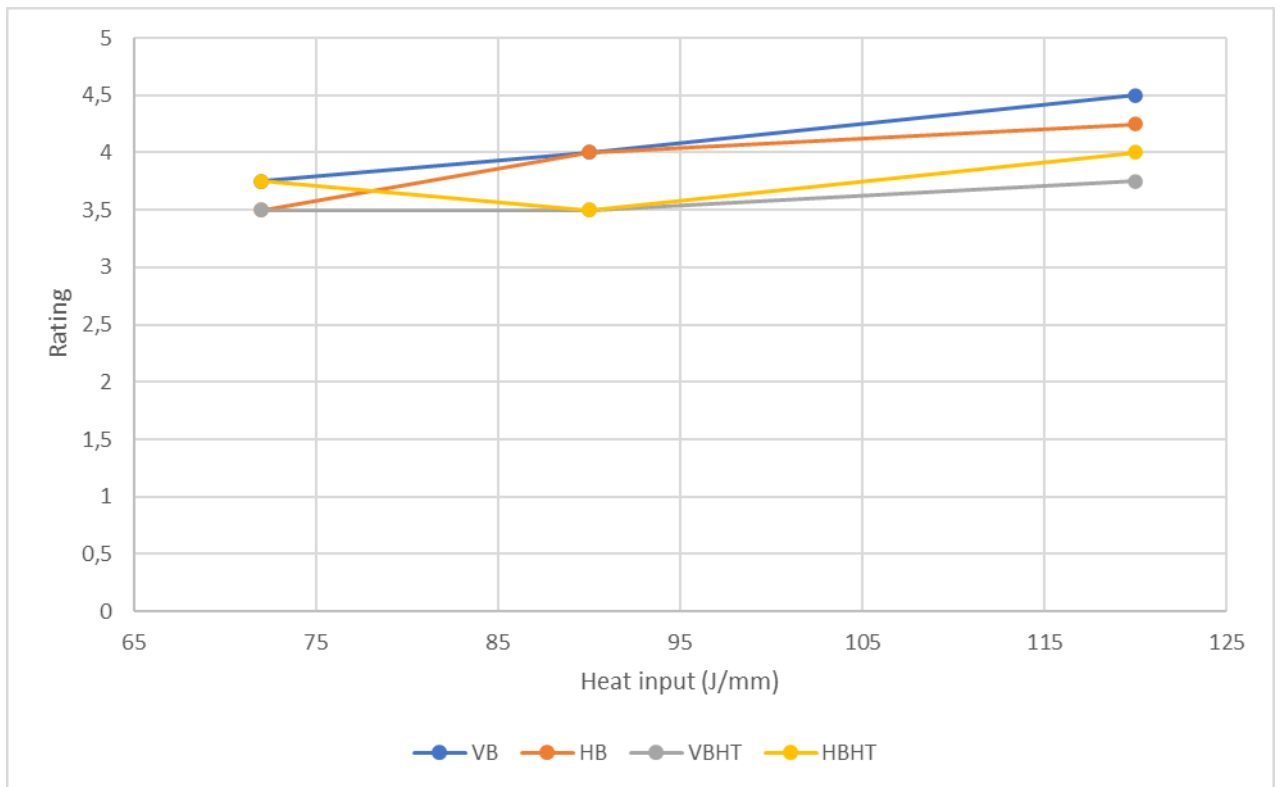


Figure 24. Overall quality, 3.0 kW welding power, welding speed 1.5 m/min, 2.0 m/min and 2.5 m/min.

For 3.0 kW laser power it can be seen that the quality of weld increases with lowering speed and increasing heat input which is the opposite result compared to 2.5 kW laser power. Here again the specimens with no heat treatment appear to have a better quality compared to heat-treated with vertical manufacturing direction having highest quality at a rating of 4.5.

Figure 25 presents overall quality for constant laser power of 3.5 kW.

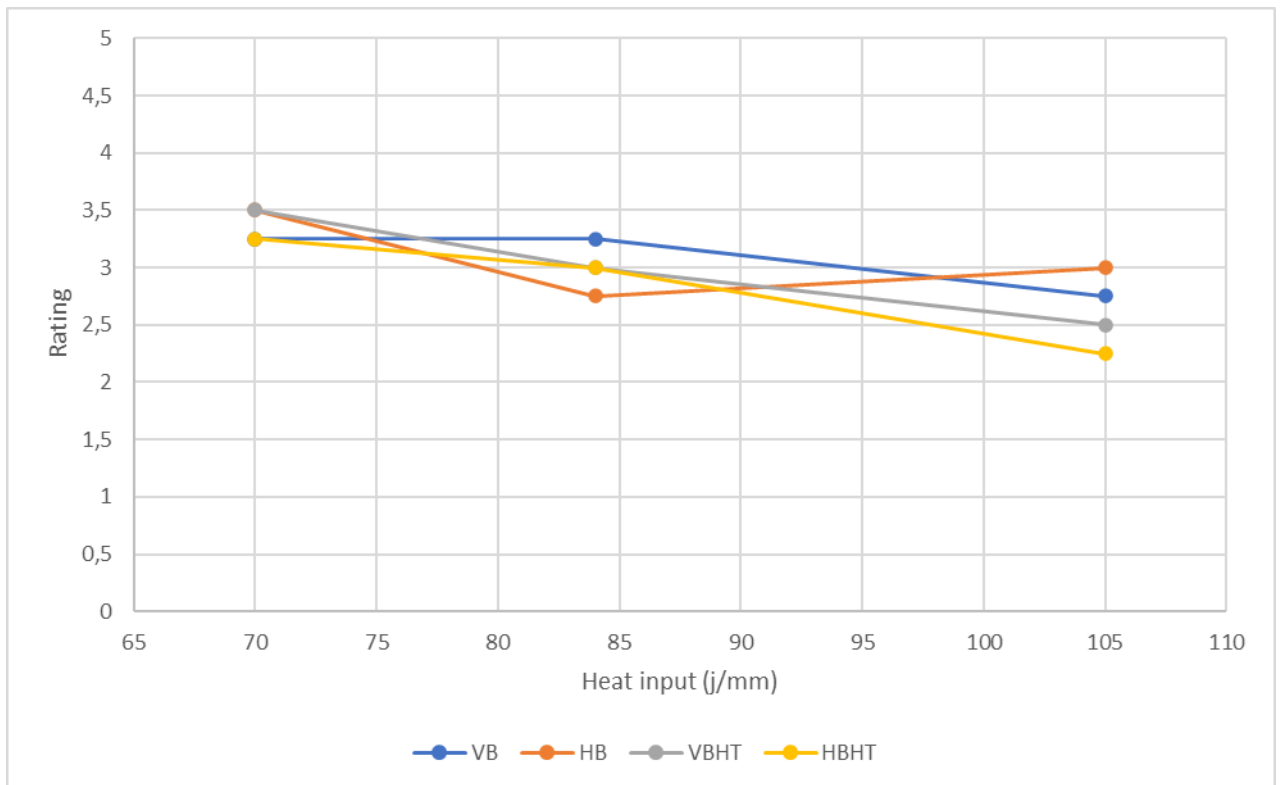


Figure 25. Overall quality, 3.5 kW welding power, welding speed 2.0 m/min, 2.5 m/min and 3.0 m/min.

At laser power of 3.5 kW the quality of weld appears to decrease with increase in heat input. However, even the best quality weld is only rated at 3.5 which is lower than the highest quality welds at lower laser powers. This would indicate that for specimens in this experiment, 3.5 kW is too much laser power and producing a high-quality weld is not reasonable. The vertically printed specimen appears to be highest quality here as well, although horizontally printed and vertically printed heat-treated specimens have the highest score of 3.5.

9.1.2 Penetration

The results for weld penetration are presented in the following figures. Penetration showed variance with welding power but overall, with lower welding power the penetration was better when compared to higher welding power.

Figure 26 presents the penetration results with 2.5 kW welding power.

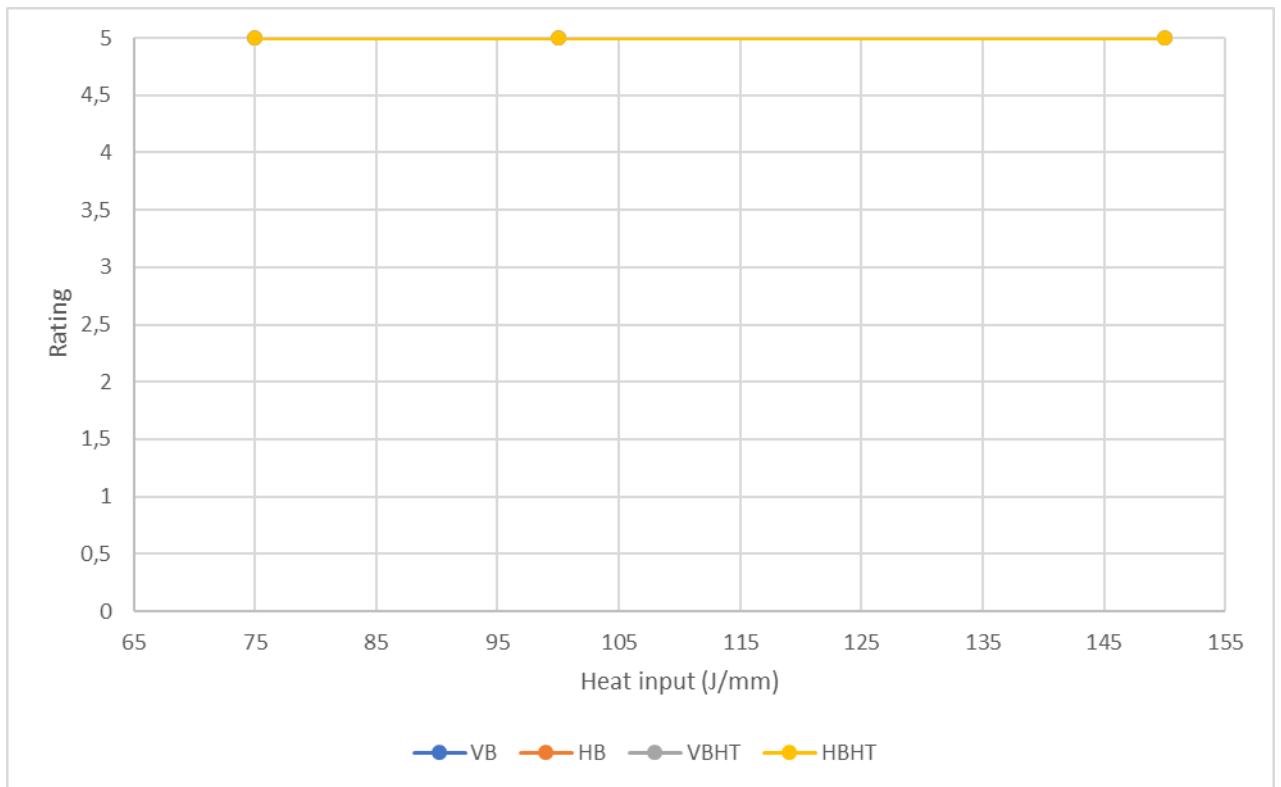


Figure 26. Penetration, 2.5 kW welding power, welding speed 1.0 m/min, 1.5 m/min and 2.0 m/min.

At 2.5 kW laser power the penetration is full penetration and good at all heat inputs. Welds also show no signs of sagging or root concavity resulting in good penetration. All welds are rated at the highest rating of 5.

Figure 27 presents the penetration results with 3.0 kW welding power.

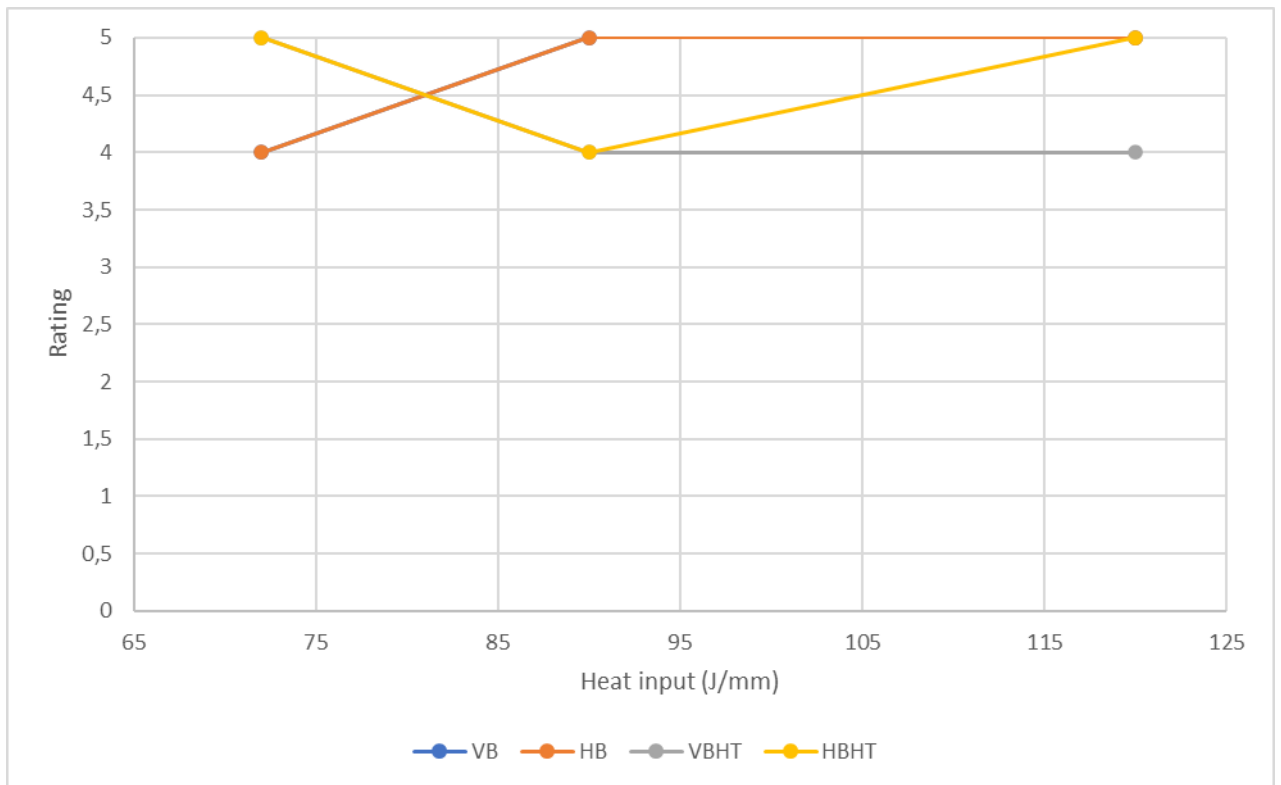


Figure 27. Penetration, 3.0 kW welding power, welding speed 1.5 m/min, 2.0 m/min and 2.5 m/min.

At 3.0 kW the welds are fully penetrated but due to sagging and root concavity the groove is slightly unfilled with certain parameter sets. For non-heat-treated specimens the quality increases with increase in heat input, whereas with heat-treated specimens the penetration quality decreases with increase in heat input. For all manufacturing directions however a rating of 5 can be found for penetration at 3.0 kW laser power. The VB curve overlaps with HB curve and VBHT curve overlaps with HBHT curve from 72 J/mm to 90 J/mm.

Figure 28 presents penetration results with 3.5 kW welding power.

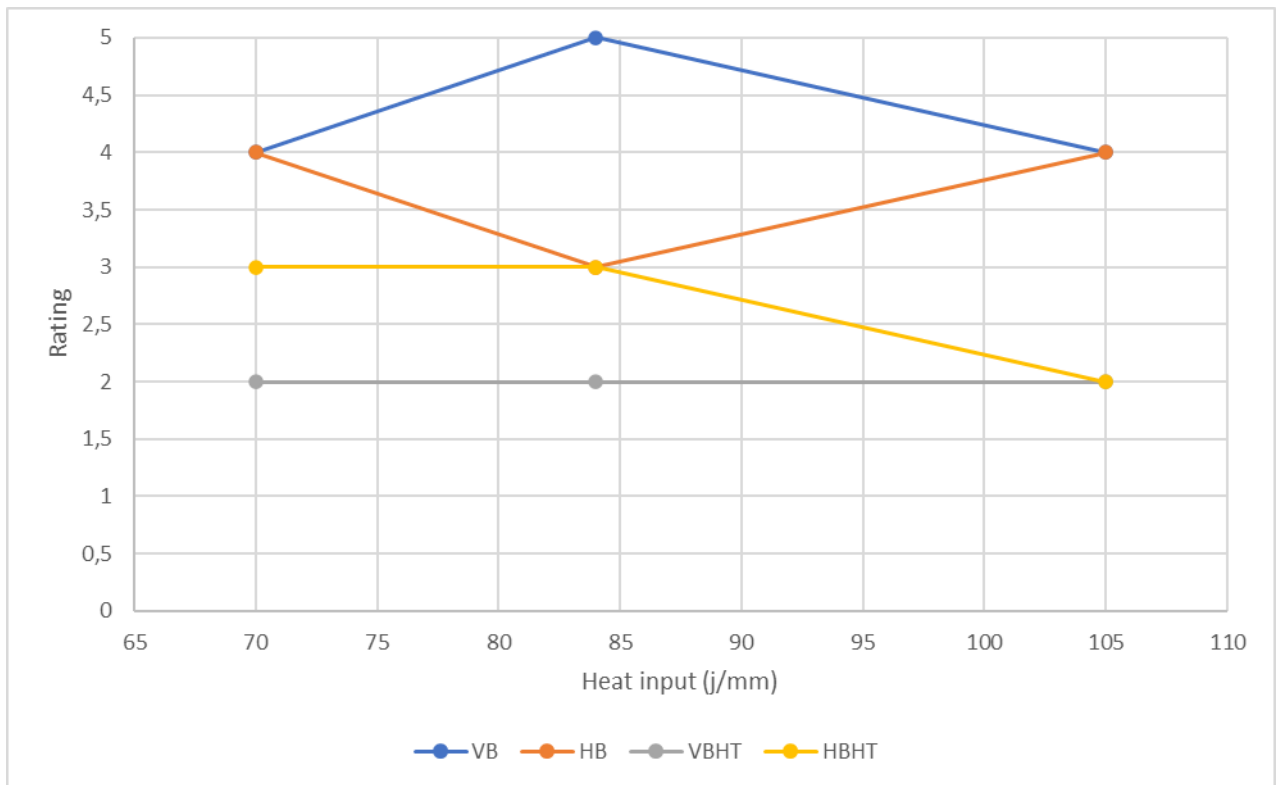


Figure 28. Penetration, 3.5 kW welding power, welding speed 2.0 m/min, 2.5 m/min and 3.0 m/min.

The welds are fully penetrated, but the weld seam shows heavy sagging and root concavity resulting in an unfilled groove. Heat treated specimens show bad penetration at all heat input rates whereas non-heat-treated are better. Vertically built specimen is rated the best at a rating of 5 at heat input of 84 J/mm. VBHT specimens show the worst penetration behavior at 3.5 kW welding power. Non-heat-treated specimens show better penetration ratings in general at 3.5 kW than heat-treated.

9.1.3 Spatter

The results for spatter ratings are shown in the next section. Overall, it was found that there is large differences in spattering depending on the parameters. With lower welding power the spattering was in general lower and as the welding power was increased, spattering also showed an increase.

Figure 29 presents the spattering results with 2.5 kW welding power.

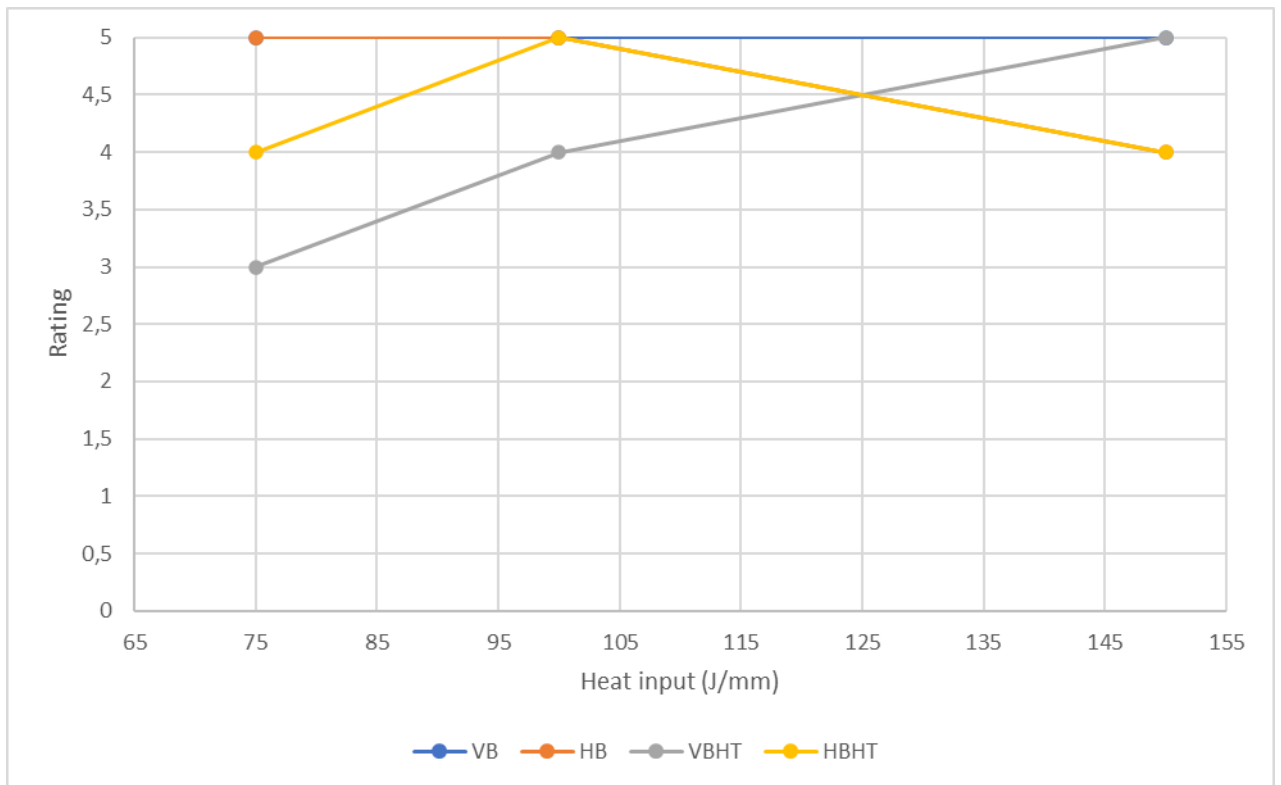


Figure 29. Spatter, 2.5 kW welding power, welding speed 1.0 m/min, 1.5 m/min and 2.0 m/min.

Figure 29 indicates that spattering at 2.5 kW is reasonable for all manufacturing types. VB specimen shows best results as spattering is rated at 5 for all heat inputs. Heat-treated specimens show more spattering at 2.5 kW than non-heat-treated specimens. The HB curve overlaps with HBHT curve from 100 J/mm to 150 J/mm and VB curve overlaps with HB curve from 75 J/mm to 100 J/mm.

Figure 30 presents the spattering results with 3.0 kW welding power.

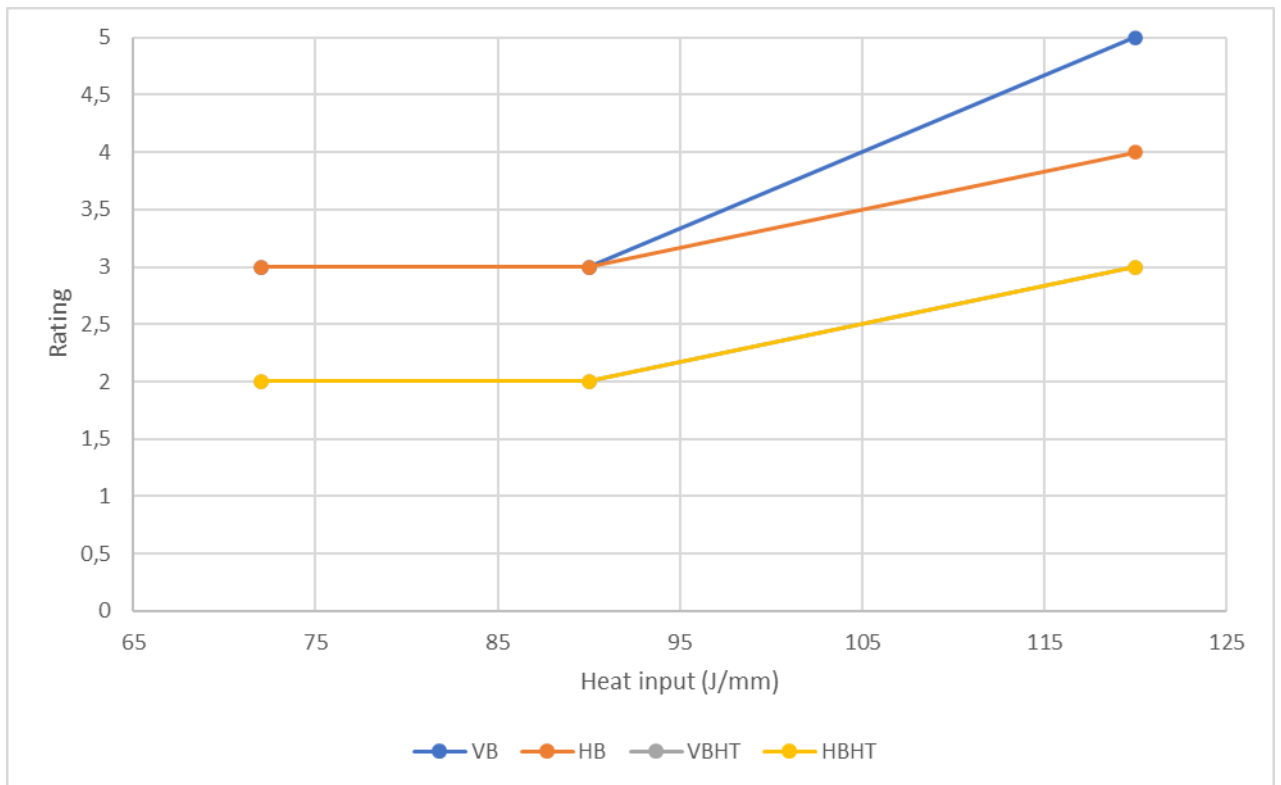


Figure 30. Spatter, 3.0 kW welding power, welding speed 1.5 m/min, 2.0 m/min and 2.5 m/min.

As it can be seen from Figure 30, at 3.0 kW laser power spattering is high at lower heat inputs and gets better as heat input is increased for all manufacturing types. The VBHT and HBHT curves overlap and show the most spattering whereas vertically manufactured scores the highest at 120 J/mm. The increase in heat input is due to lowering of the welding speed which appears to decrease spattering and improve the quality of the weld. The weld pool with a lower speed stays more stable and melting is more complete which may be the reason for less spattering.

Figure 31 presents the spattering results for 3.5 kW welding speed.

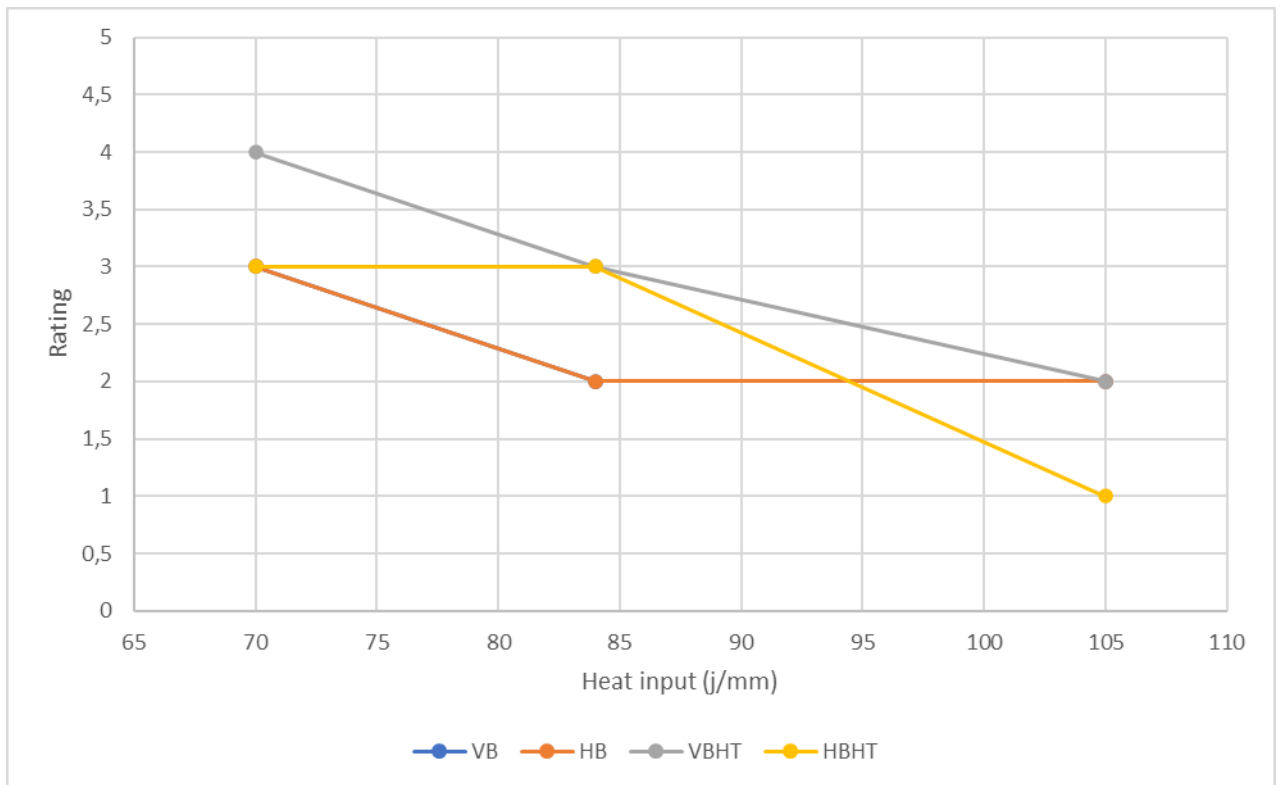


Figure 31. Spatter, 3.5 kW welding power, welding speed 2.0 m/min, 2.5 m/min and 3.0 m/min.

At 3.5 kW spattering is at a reasonable level with low heat inputs but very bad at higher heat inputs. Horizontally and vertically manufactured curves are overlapping. At this laser power, the VBHT specimens show the best quality in terms of spattering and non-heat-treated specimens score the lowest. VB and HB curves overlap. Opposite of what happens with 3.0 kW welding power, the rating is lower with higher heat input. This suggests that if spattering needs to be avoided, with a higher laser power faster welding speed should be used and vice versa with lower welding power. The sample size is not large however and further studies should be conducted to fully understand the causes of spattering.

9.1.4 Root quality

Root quality of specimens is examined in this section. Root quality varied between ratings 1 and 5 and therefore requires the optimal parameters. With a lower welding power, the root quality was in general better.

Figure 32 presents the root quality results for 2.5 kW welding power.

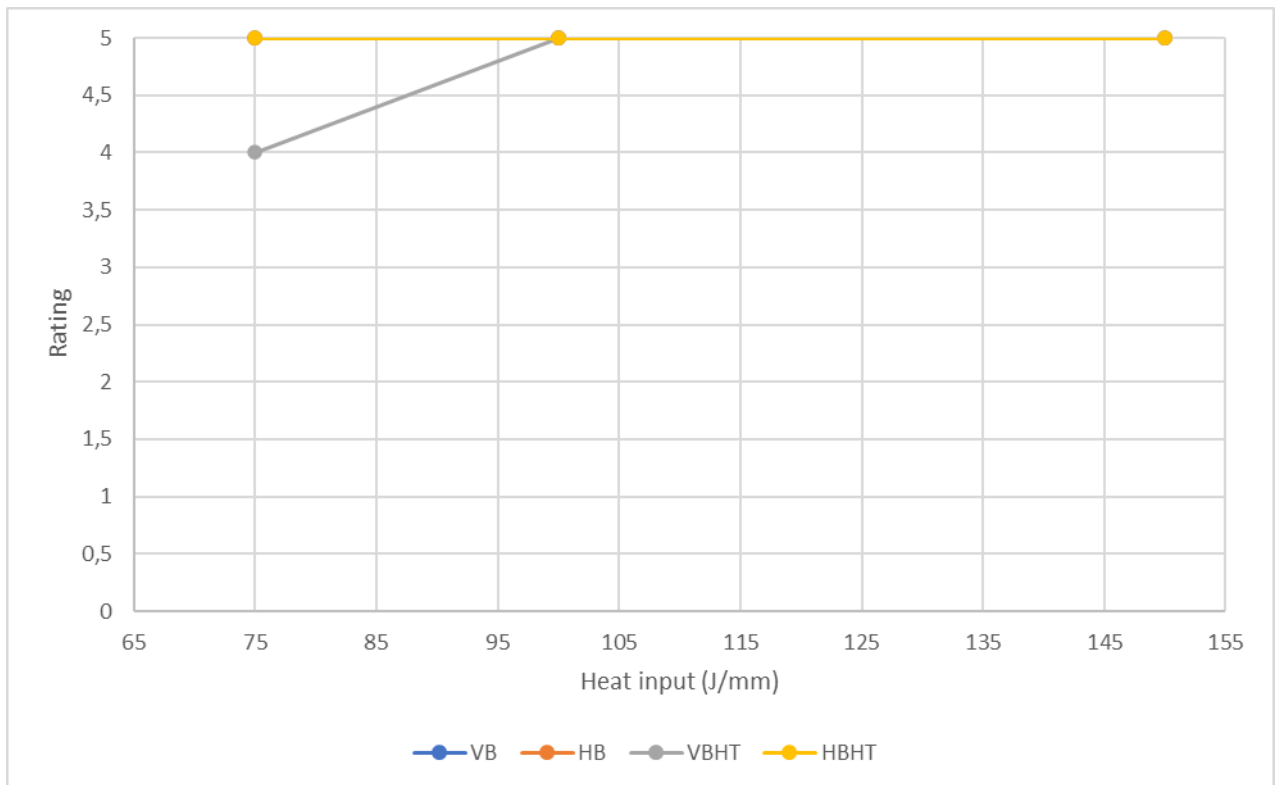


Figure 32. Root quality, 2.5 kW welding power, welding speed 1.0 m/min, 1.5 m/min and 2.0 m/min.

At 2.5 kW the root quality of very good at all heat inputs. VBHT specimen at low heat input shows a decrease in quality of root, but overall, very good root quality at all heat inputs. This suggests that a low welding power is key to a good quality root. Welding speed and heat input do not affect the root quality as much.

Figure 33 presents the root quality results for 3.0 kW welding power.

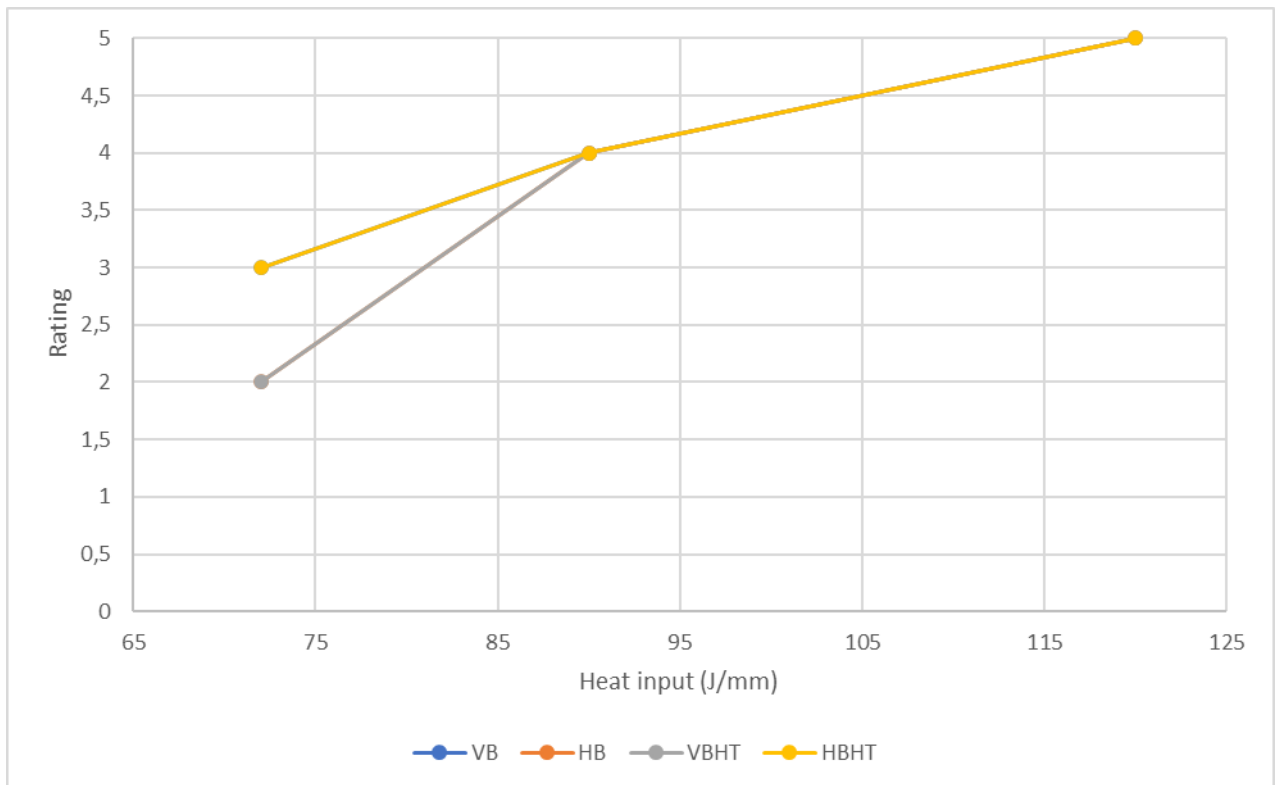


Figure 33. Root quality, 3.0 kW welding power, welding speed 1.5 m/min, 2.0 m/min and 2.5 m/min.

At 3.0 kW laser power the root quality of all specimens appears to increase with a higher heat input suggesting that at this power level a higher heat input is better for root quality. Results clearly show that comparing with 2.5 kW laser power the root quality is decreased, however increases with higher heat input. It seems that a higher heat input overall improves root quality.

Figure 34 presents the root quality results for 3.5 kW welding power.

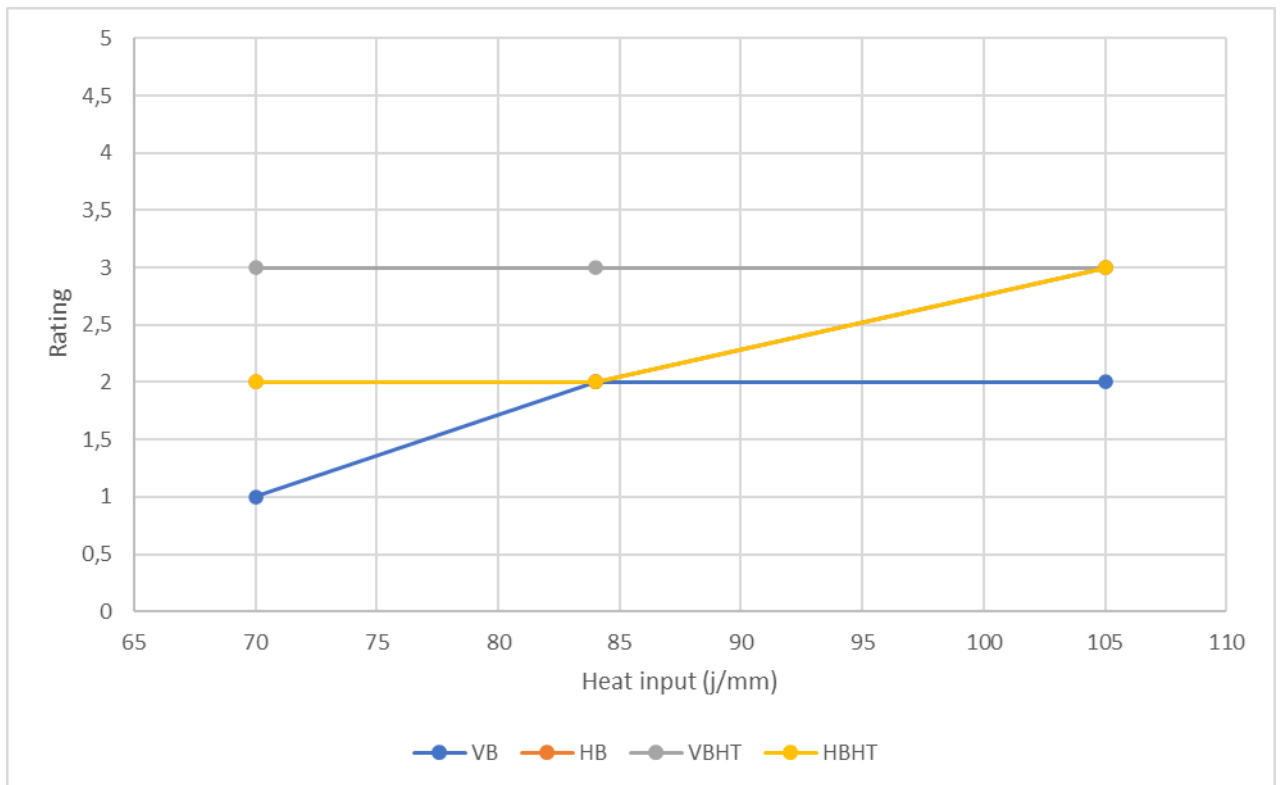


Figure 34. Root quality, 3.5 kW welding power, welding speed 2.0 m/min, 2.5 m/min and 3.0 m/min.

At the highest laser power of 3.5 kW the root quality ranges from 1 to 3 which is lower than in the lower laser power ranges. This suggests that for root quality 3.5 kW is too high power. The vertically built heat-treated specimens behave the best at this higher power with a rating of 3 through all heat inputs. VB specimen performs the worst with rating ranging from 1 to 2. HB and HBHT curves overlap. It was observed that with the lower welding powers results in better root quality than with the highest power of 3.5 kW.

9.1.5 Heat affected zone.

Heat affected zone results are presented. In general, a higher heat input results in a larger HAZ and that was also observed in the experiments. It was also examined that the welding power alone does not have a significant effect on the size of the HAZ, but heat input affects more. The larger the HAZ the lower the score.

Figure 35 presents the HAZ results for 2.5 kW welding power.

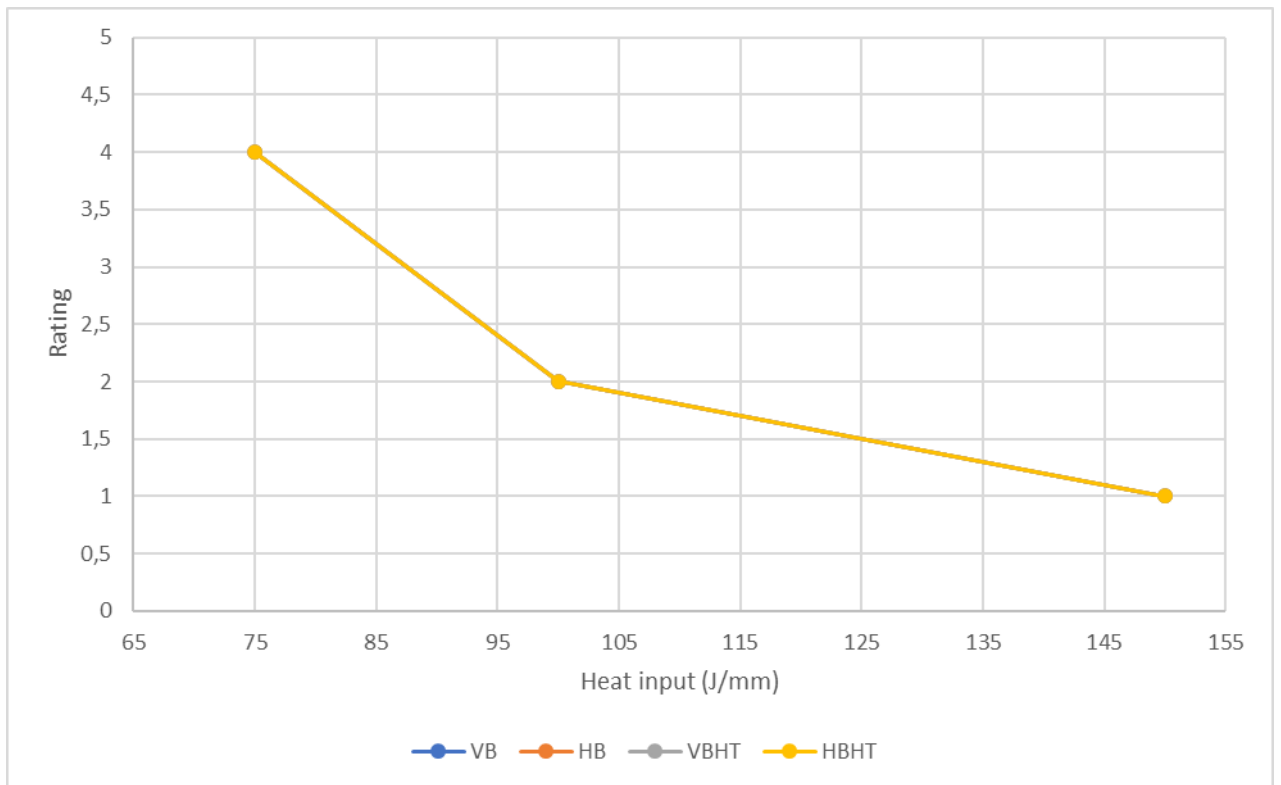


Figure 35. HAZ, 2.5 kW welding power, welding speed 1.0 m/min, 1.5 m/min and 2.0 m/min.

The HAZ at 2.5 kW rates between 4 and 1. As expected, when heat input is higher the HAZ is larger and therefore worse. Tests at 2.5 kW welding power were at slower welding speeds as well which results in a larger HAZ. The weld rated at 1 for HAZ is the weld with the lowest welding speed and highest heat input out of all tests and therefore the largest HAZ.

Figure 36 presents the HAZ results for 3.0 kW welding power.

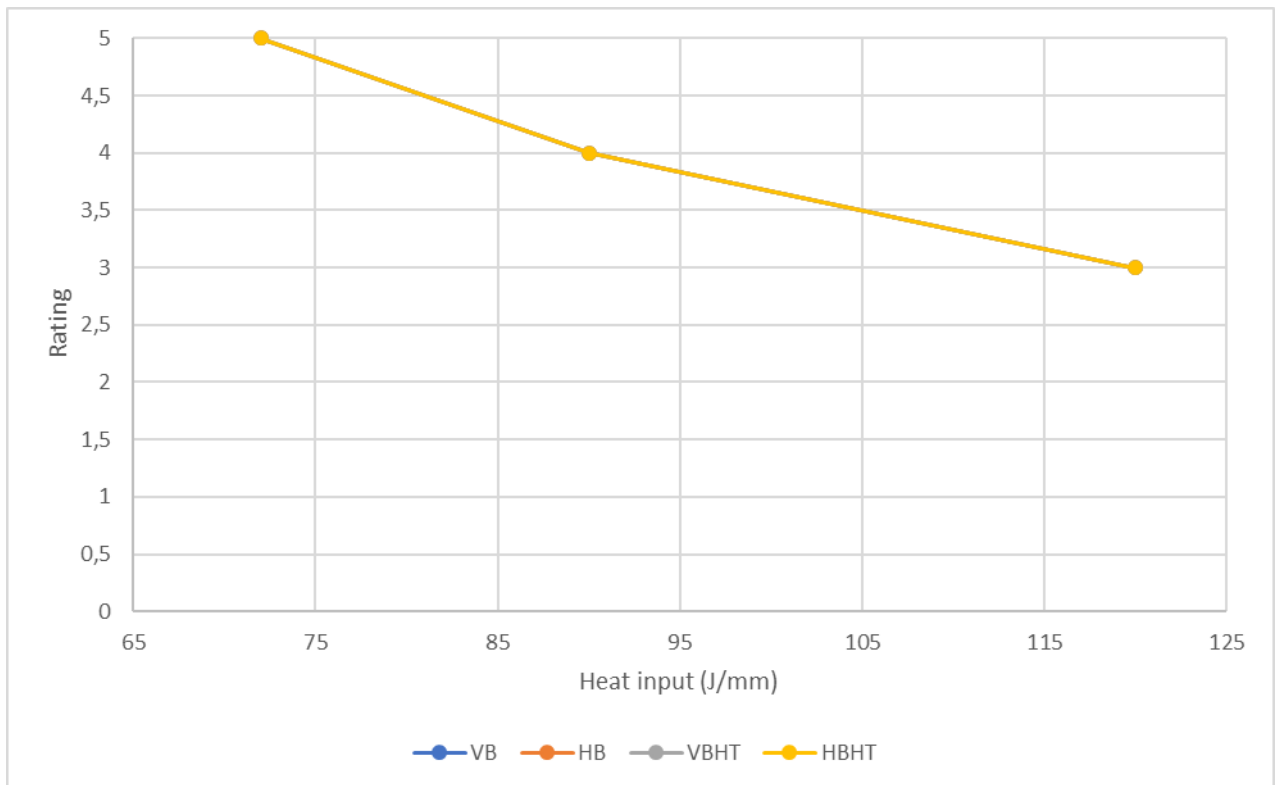


Figure 36. HAZ, 3.0 kW welding power, welding speed 1.5 m/min, 2.0 m/min and 2.5 m/min.

HAZ ranges between 5 and 3 rating and 3.0 kW with better results at lower heat inputs. Overall good HAZ at 3.0 kW. Results are quite as expected; when heat input is high the width of the HAZ increases as heat is what causes the formation of the HAZ. It is noticeable however that HAZ scores better with 3.0 kW than with 2.5 kW welding power. This could mean that the faster welding speeds used at this welding power help in keeping the HAZ smaller.

Figure 37 presents the results for 3.5 kW welding power.

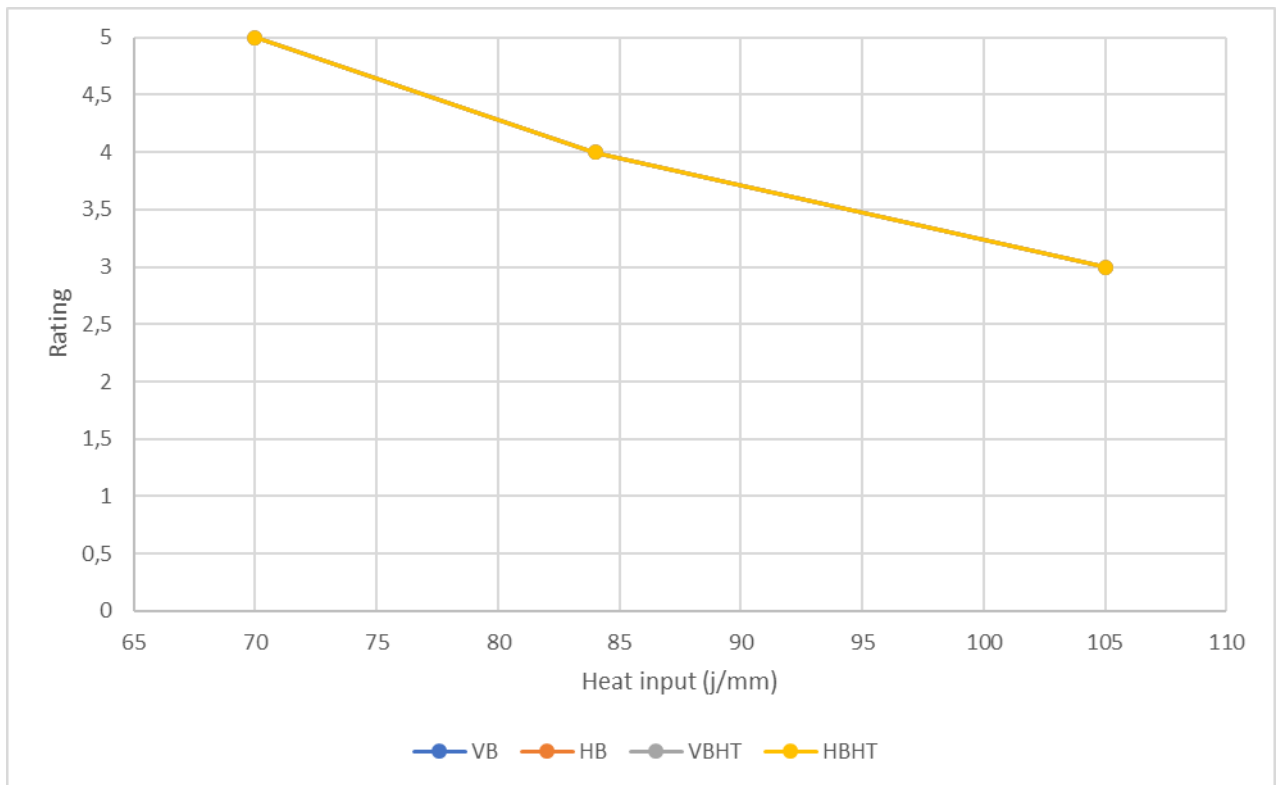


Figure 37. HAZ, 3.5 kW welding power, welding speed 2.0 m/min, 2.5 m/min and 3.0 m/min.

Similar results are rated for HAZ at 3.5 kW as at 3.0 kW. Overall good. The faster welding speeds used when testing at 3.5 kW also help with achieving a smaller HAZ. As the results show, HAZ is better with higher welding powers. This seems to indicate that the welding power is not affecting the HAZ as much as welding speed which is faster with higher welding powers. To have good HAZ in the weld it would seem that higher welding power with higher welding speed is beneficial.

9.2 Results of weld cross-section geometry

Results of weld cross-section geometry are presented. Overall, it was observed that a higher heat input resulted in a wider weld cross-section which is reasonable as the melt pool is larger with higher heat input. The graphs are presented for top, middle and bottom measurements.

Figure 38 presents the results for weld cross-section width from the top.

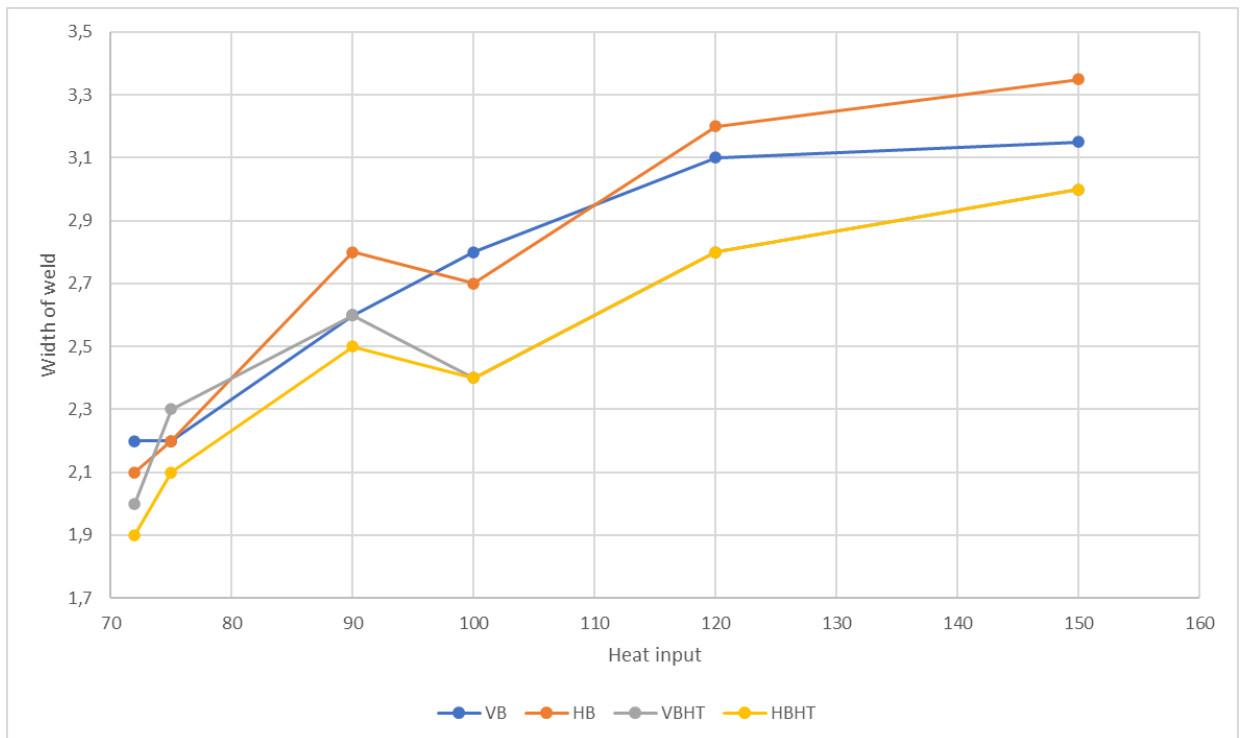


Figure 38. Width of weld measured from the top.

As Figure 38 presents the width of the weld increases with the increase in heat input. The increase is very similar regardless of printing direction, but it needs to be noticed that with heat treatment the weld is narrower than without heat treating the AM specimens. This suggests the heat treatment prior to welding helps in achieving a narrower weld. The weld cross section is widest when the building direction is parallel to welding direction.

Figure 39 presents the results for weld cross-section width from the middle.

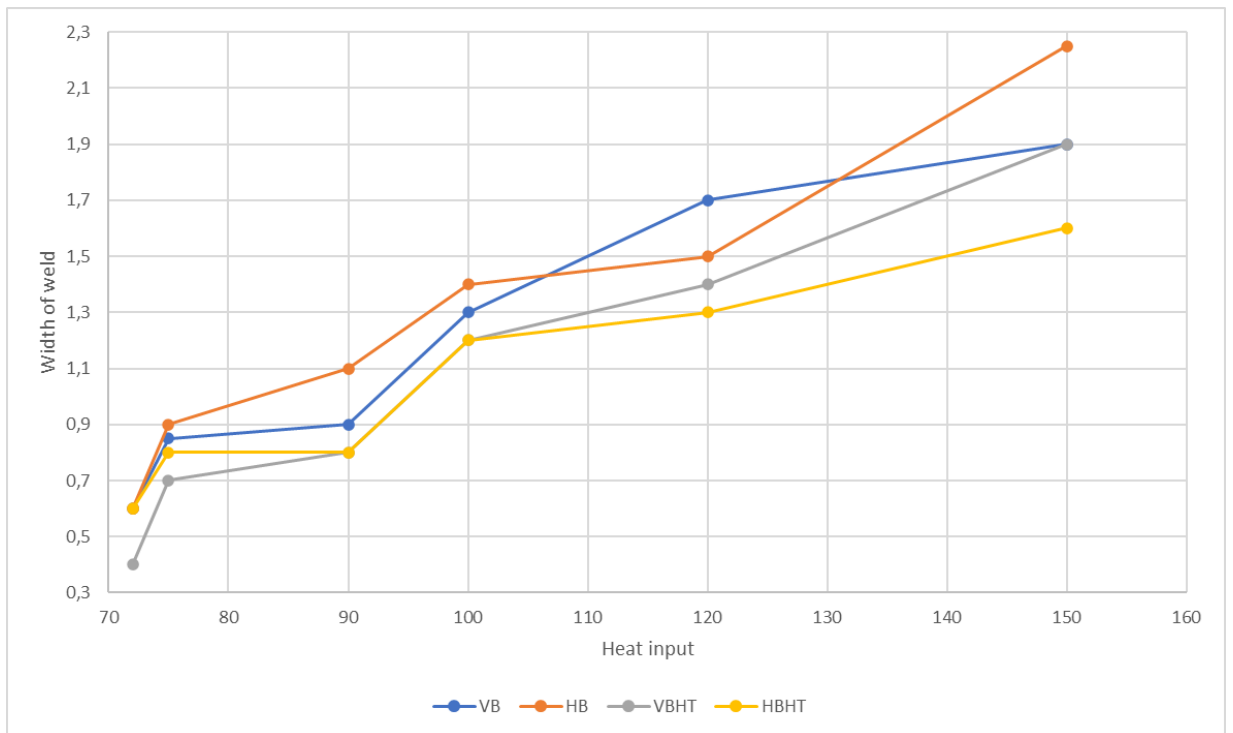


Figure 39. Width of weld measured from the middle.

Figure 39 shows similar results as Figure 38. Heat treated specimens have a narrower width in the weld and the horizontally manufactured specimens are the widest. Welds are the narrowest in the middle and wider at the top and bottom.

Figure 40 presents the results for weld cross-section width from the top.

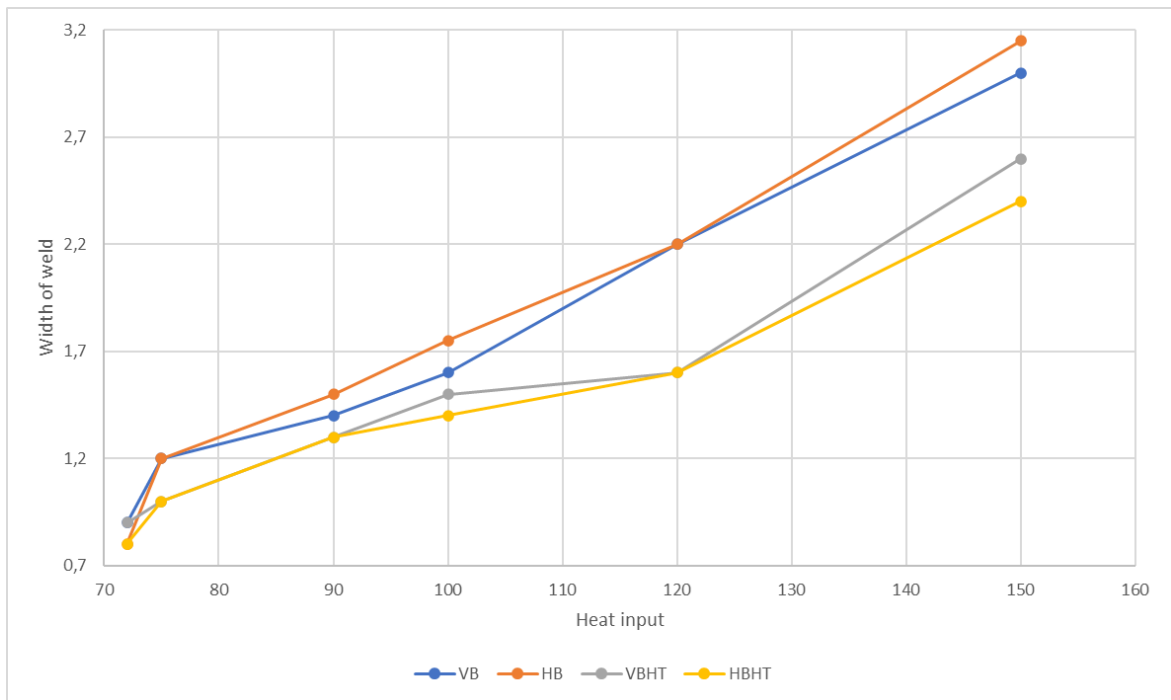


Figure 40. Width of weld measured from the bottom.

In summary, the weld widths were measured from the top, middle, and bottom and all measurements show similar results. Horizontally manufactured specimens have the widest welds and heat-treated specimens have the narrowest welds. This also indicates that increasing the heat input increases the size of the HAZ also, and this is proven by the visual inspection results presented in Figure 41.

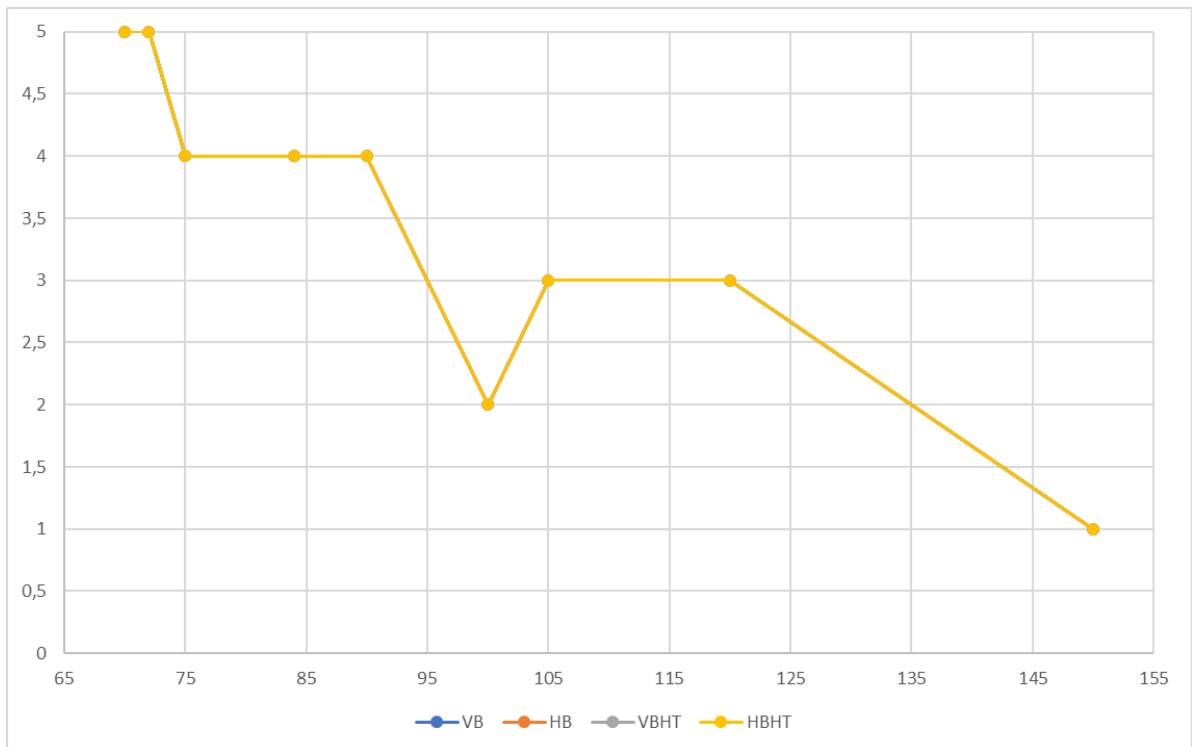


Figure 41. Visual inspection of HAZ with increasing heat input.

Figure 41 shows the results of visual inspection of HAZ. The higher the score, the smaller the HAZ. It can be seen that by increasing heat input, the HAZ size increases which corresponds with the results of the width measurement data. It should also be noted that the manufacturing method has little to no effect on the size of the HAZ.

9.3 Imperfections

Imperfections found in welds were assessed based on standard SFS-EN ISO 13919-1 Electron and laser-beam welded joints. Requirements and recommendations on quality levels for imperfections. Part 1: Steel, nickel, titanium, and their alloys. The standard rates imperfections to three categories; D, C and B. B being the best and D being the worst. (SFS-EN ISO 13919-1 2019, p. 8)

9.3.1 Root concavity

Root concavity is found in a number of welds. Most common cause for root concavity is the root gap being either too small or too large. Also, high welding speed can cause root concavity. (TWI-Global 2004)

Figure 42 presents an example of root concavity.

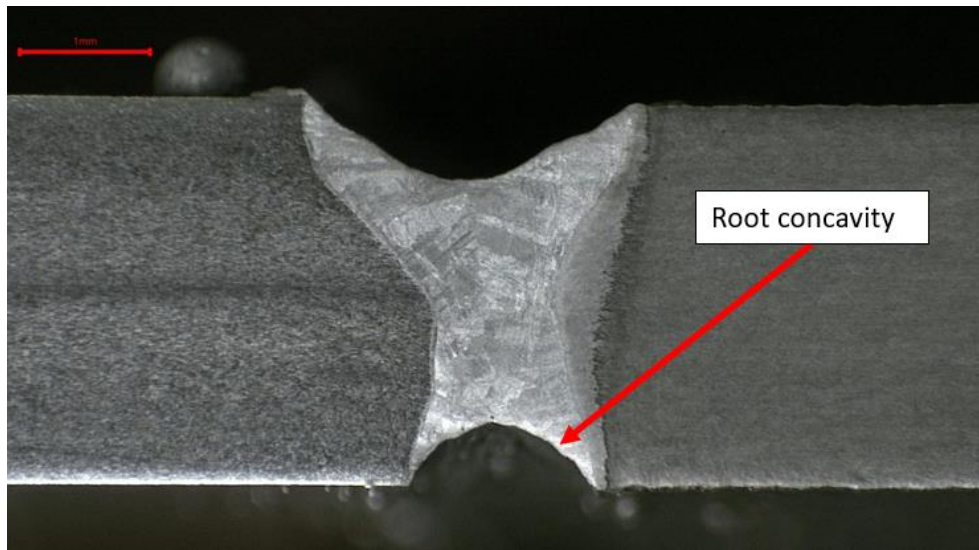


Figure 42. Root concavity of the weld cross-section.

As figure 42 shows, in this weld the root concavity is clearly visible. As mentioned, high welding speed can cause root concavity and that is visible in the tests. The highest welding speeds of 2.5 m/min to 3.0 m/min show the most root concavity.

There are also differences between manufacturing methods. Heat-treated specimens show more root concavity than non-heat-treated specimens. Vertically built non-heat-treated specimens show the least root concavity. Figure 43 shows how root concavity rated for each welding parameter set.

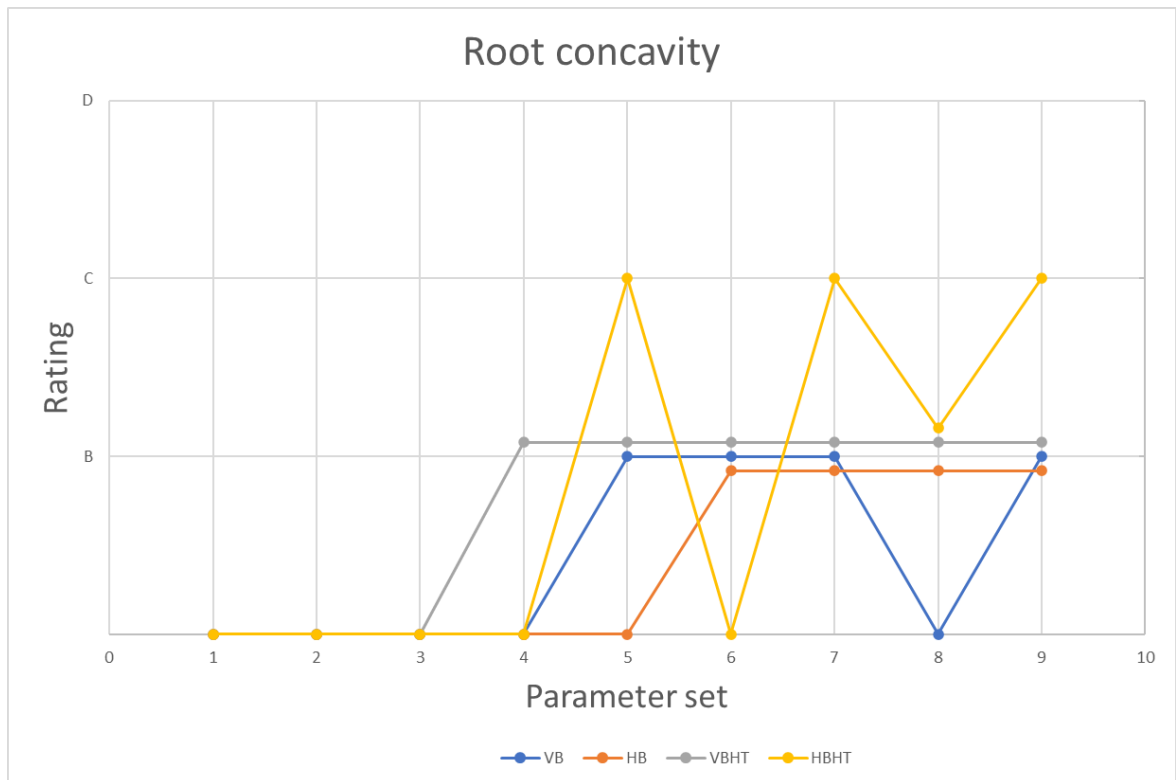


Figure 43. Root concavity with all parameter sets.

As the figure shows, HBHT rates worst for root concavity. Generally, the combination of high welding speed and high welding power with heat treatment results in more root concavity than lower welding speed and welding power. Since root gap preparation before welding is a common cause for root concavity, the joint preparation might be a cause as well.

9.3.2 Sagging

Sagging, or incompletely filled groove, is an imperfection similar to root concavity but on the top side of the weld. As with root concavity sagging is often caused by excessive welding speed. (TWI-Global 2004)

Figure 44 presents an example of sagging in weld.

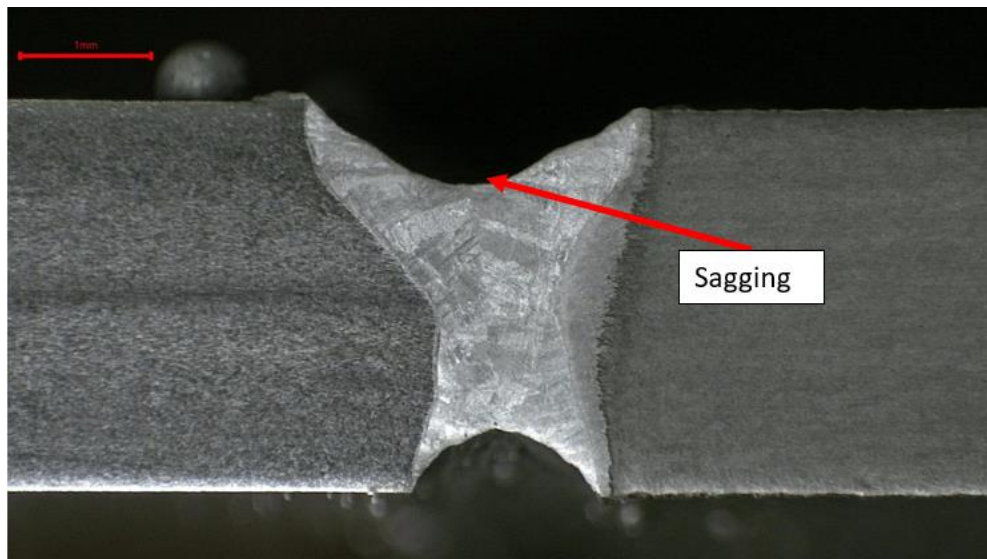


Figure 44. Sagging of the weld cross-section.

As can be seen from figure 44, sagging is clearly visible. Sagging was found mostly with high welding power combined with high welding speed. It was also found that sagging was almost non-existent in specimens without heat treatment and common in heat-treated specimens. This suggests that heat-treated specimens are more prone to sagging than non-heat treated. Figure 45 shows an example of this with parameter set 9 from Table 8.

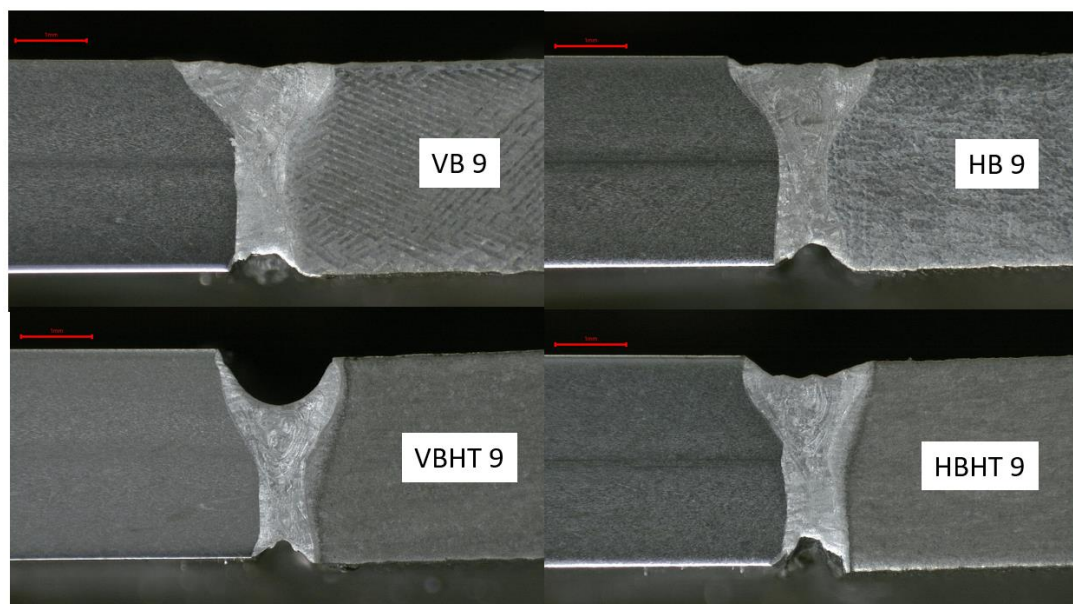


Figure 45. Comparison of sagging with different building parameters

As the figure shows, specimens without heat-treatment show no to very little sagging. Heat-treated specimens however show clear sagging with both building directions. Vertically built heat-treated has the most unfilled groove. This may result from the microstructural changes that occur with the heat-treatment, but more studies are needed to fully determine why this occurs.

Figure 46 presents how sagging results are with different parameter sets.

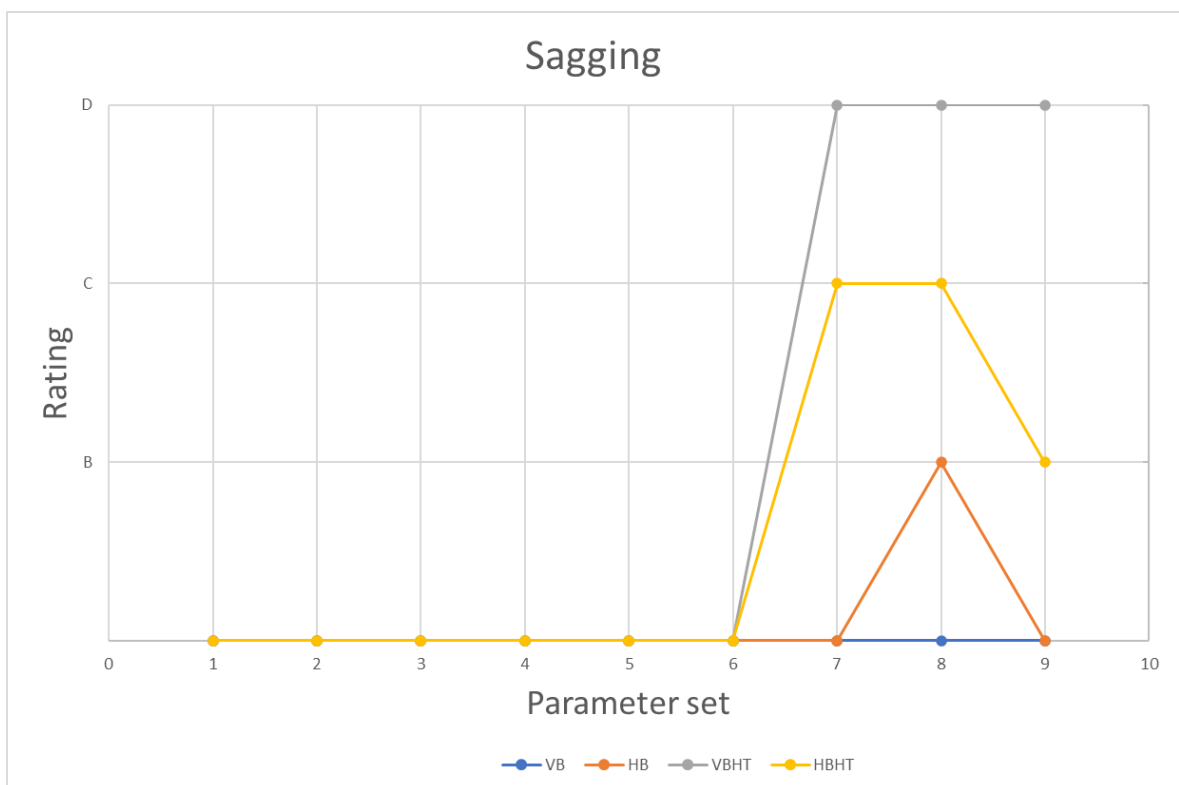


Figure 46. Sagging with all parameter sets.

As figure 46 shows, heat-treated specimens show high sagging compared to non-heat treated. As in root concavity, the combination of high welding speed, high welding power and heat treatment makes the weld more prone to sagging.

Based on the results of this thesis the optimal welding parameters are listed in table 10.

Table 10. Optimal welding parameters for IN718 to 316L steel

| Building | Welding power [kW] | Welding speed [m/min] | Heat input [J/mm] | Overall quality |
|-----------------|-------------------------------|----------------------------------|------------------------------|----------------------------|
| VB | 2.5 | 2.0 | 75 | 4.75 |
| HB | 2.5 | 2.0 | 75 | 4.75 |

As table 10 shows, the VB and HB building methods resulted in the best overall quality rating of 4.75. It can be noticed that the best overall quality was reached with the lowest welding power used in the experiments of 2.5 kW, 2.0 m/min welding speed and heat input of 75 J/mm. This indicates that lower heat input is optimal in reaching a high-quality weld. The highest score of 4.75 was only reached with specimens without heat-treatment. It was noted with nearly all the rating categories that lower heat input was better for the quality. Only the HAZ scored a 4 instead of 5 due to the heat input not being the lowest out of all tests. In general, with the above parameters a good quality weld based on visual inspection can be achieved.

10 CONCLUSIONS

L-PBF and AM in general is a promising manufacturing method for the future. It provides means to design products and components in a totally new way as it allows a completely new level of optimization for the design process and flexibility for the manufacturing process. AM allows the complete optimization of parts and products to their specific needs and simplifies the manufacturing process. AM and L-PBF in particular comes with its limitations as well. Part size is a big limitation as the current range of L-PBF machines only allows the size of the produced parts to be no bigger than the build chamber of the machines. This is the reason why welding of L-PBF parts needs to be researched to allow for L-PBF parts to be combined and form bigger end products when necessary.

This thesis was conducted with the Laser Material Processing and Additive Manufacturing research group of LUT University. The aim of the thesis was to study the weldability of AM IN718 and wrought 316L steel and the effect of different building and welding parameters and to find the optimal parameters. The evaluation of the welds was carried out through visual inspection of the welds and by evaluating the microscopic images of the cross-sections of the welds.

The thesis was carried out in two parts. Firstly, a literature review of previous studies in the area and through an experimental part where welds were carried out in the laser processing laboratory at LUT University. The literature review was done to figure out how the welding was done in previous studies and to get an idea for the welding parameters. Experimental part was conducted to more specifically study the dissimilar joint between wrought 316L and AM IN718.

The amount of research in the area of welding L-PBF parts is not high. This indicates that further studies are needed. However, some conclusions from the found articles could be made. Most importantly previous studies showed that the welding of L-PBF parts can be done. The L-PBF process means that the finished parts are somewhat different from traditionally manufactured metal parts, but it doesn't have a big impact on weldability. The building direction affected the quality of the welds somewhat and should be considered when welding L-PBF parts.

Experimental part was set up to examine the weld in more detail and to be able to study how different building and welding parameters affect the weld. Laser welding was selected as the welding process. Similar conclusions could be made from the experiments as the literature review already showed. The specimens of 316L and AM IN718 showed overall good weldability and welding was successful. It was noted that building parameters, such as heat-treatment and building direction, did affect the weld quality and should be considered. Welding parameters also had an affect but with the optimal parameters the weld quality was good.

Overall, it was determined that weldability of 316L and AM IN718 is found good. Weld quality assessed with visual inspection showed that with the right parameters imperfections can be avoided. For future studies more focus should be put towards researching in more detail how the building direction affects the quality of the weld. With the limited sample size of this thesis, it could be seen that it had an effect, but the scale is difficult to determine. It can be said however that L-PBF produced parts have good laser weldability and it is a viable option to join parts to form larger end products.

11 FURTHER STUDIES

As the results of this thesis show, specimens of AM IN718 and wrought 316L can be welded together. Based on results of visual inspection and microscopic images of the weld seam a good quality weld can be done with optimized parameters. This thesis did not however include tensile testing or any other destructive testing of the welded specimens to further test and verify the quality and strength of the welds which could be done in a further study to confirm the quality and strength of the welds.

The AM direction also influenced the quality of welds. In some evaluation criteria results were similar but differences could be seen between vertically built and horizontally built. Further studies could be conducted to further research how big an effect the building direction has on the weld quality and strength. It is an important aspect to know whether it is another parameter that needs to be considered when producing L-PBF parts that are meant to be welded.

Effect of heat-treatment could also be studied in more detail. It was observed that it influenced the quality of the weld and especially in some imperfections it seemed that heat-treated specimens were more prone to certain imperfections.

LIST OF REFERENCES

Biffi, C.A., Fiocchi, J. & Tuissi, A. 2019. Laser weldability of AlSi₁₀Mg alloy produced by selective laser melting: Microstructure and mechanical behavior. *Journal of Materials Engineering and performance*, vol 28. pp. 6714-6719.

Brandt, M. 2017. *Laser additive manufacturing: Materials, design, technologies, and applications*. Amsterdam: Elsevier. 479 p.

Diegel, O., Nordin, A. & Motte, D. 2019. *A Practical Guide to Design for Additive Manufacturing*. Singapore: Springer. 226 p.

EOS NickelAlloy IN718. 2020. Material Data Sheet. [web document]. [Referred 10.2.2021]. Available: <https://www.eos.info/en/additive-manufacturing/3d-printing-metal/dmls-metal-materials/nickel-alloys>

Hawk, C. 2019 Laser welding behavior of laser powder bed fusion additive manufactured 304L stainless steel. Doctoral thesis. Colorado School of Mines. 258 p.

Hong, J.K., Park, J.H., Park, N.K., Eom, I.S., Kim, M.B. & Kang, C.Y. 2008. Microstructures and mechanical properties of Inconel 718 welds by CO₂ laser welding. *Journal of Materials Processing Technology*, vol. 201. pp. 515-520.

Janicki, D.M. 2015. Fiber laser welding of nickel based superalloy Inconel 625. *Proceedings of SPIE – Laser Technology 2012: Applications of Lasers*, vol 8703. pp. 87030R-1 - 87030R-6

Karayel, E. & Bozkurt, Y. 2020. Additive manufacturing method and different welding applications. *Journal of Materials Research and Technology*. pp. 11424-11438.

Katayama, S. 2013. *Handbook of laser welding technologies*. 632 p.

Milewski, J.O. 2017. Additive Manufacturing of Metals. From Fundamental Technology to Rocket Nozzles, Medical Implants, and Custom Jewelry. Cham: Springer. 343 p.

Mohyla, P., Hajnys, J., Sternadelova, K., Krejci, L., Pagac, M., Konecna, K. & Krpec, P. 2020. Analysis of Welded Joint Properties on an AISI316L Stainless Steel Tube Manufactured by SLM Technology. *Materials* 2020, vol. 13. pp. 1-14.

Prabaharan, P., Devendranath Ramkumar, K. & Arivazhagan, N. 2014. Characterization of microstructure and mechanical properties of Super Ni 718 alloy and AISI 316L dissimilar weldments. *Materials Research Society* 2014, pp. 3011-3023.

Raza, T. 2020. Process understanding and weldability of laser-powder bed fusion manufactured alloy 718. 146 p.

SFS-EN ISO 13919-1. 2019. Electron and laser-beam welded joints. Requirements and recommendations on quality levels for imperfections. Part 1: Steel, nickel, titanium, and their alloys. Finnish standard association. Helsinki. 23 p.

Sharma SK., Biswas K., Nath AK., Manna I. & Dutta Majumdar J. 2020. Microstructural Change during Laser Welding of Inconel 718. *Optik – International Journal for Light and Electron Optics*, vol. 218. pp. 1-11.

Special Metals. 2017. Inconel alloy 718. [web document]. [Referred 12.2.2021]. Available: http://www.specialmetals.com/assets/smc/documents/inconel_alloy_718.pdf

Strößner, J., Terock, M., Glatzel, U. 2015. Mechanical and Microstructural Investigation of Nickel-Based Superalloy IN718 Manufactured by Selective Laser Melting (SLM). *Advanced Engineering Materials*. pp. 1099-1105.

ThoughtCo. 2020. Type 316 and 316L stainless steels. [web document]. [Referred 12.2.2021] Available: <https://www.thoughtco.com/type-316-and-316l-stainless-steel-2340262>

TWI-Global. 2004. A general review of geometric shape imperfections – Types and causes Part 1 & Part 2. [web document]. [Referred 15.2.2021]. Part 1 available: <https://www.twi-global.com/technical-knowledge/job-knowledge/a-general-review-of-geometric-shape-imperfections-types-and-causes-part-1-067>. Part 2 available: <https://www.twi-global.com/technical-knowledge/job-knowledge/a-general-review-of-the-causes-and-acceptance-of-shape-imperfections-part-2-068>

Voropaev, A., Stramko, M., Sorokin, A., Logachev, I., Kuznetsov, M. & Gook, S. 2020. Laser welding of Inconel 718 nickel-based alloy layer-by-layer products. *Materials Today: Proceedings*, vol. 30. pp. 473-477.

Wits, W.W. & Jauregui Becker, J.M. 2015. Laser beam welding of titanium additive manufacture parts. 3rd CIRP Global web conference. pp. 70-75.

Wohlers, T., Campbell, I., Diegel, O., Hugg, R., Kowen, J., Bourell, D.L., Ismail, F. & Sander, P. 2020. Wohlers report 2020. 3D printing and additive manufacturing state of the industry. 383 p

Yang, J., Wang, Y., Li, F., Huang, W., Jing, G., Wang, Z. & Zeng, X. 2019. Weldability, microstructure, and mechanical properties of laser-welded selective laser melted 304 stainless steel joints. *Journal of Materials Science & Technology*. pp. 1817-1824.

Yang, L., Hsu, K., Baughman, B., Godfrey, F., Medina, F., Menon, M. & Wiener, S. 2017. *Additive Manufacturing of Metals: The Technology, Materials, Design and Production*. Cham: Springer. 168 p.

Yu, H., Li, F., Yang, J., Shao, J., Wang, Z. & Zeng, X. 2018. Investigation on laser welding of selective laser melted Ti-6Al-4V parts: Weldability, microstructure and mechanical properties. *Materials Science & Engineering*. pp. 20-27.

Zapf, H., Höfemann, M. & Emmelmann, C. 2020. Laser welding of additively manufactured medium manganese steel alloy with conventionally manufacture dual-phase steel. 11th CIRP Conference on Photonic Technologies. pp. 655-660.

Table 11. Parameter sets for visual inspection examples.

| | | Power [kW] | Speed [m/min] | Heat input [J/mm] |
|-----------------|---|------------|---------------|-------------------|
| Overall quality | 1 | 3.0 | 2.0 | 90 |
| | 5 | 2.5 | 2.0 | 75 |
| Penetration | 1 | 3.5 | 3.0 | 70 |
| | 5 | 2.5 | 1.0 | 150 |
| Spatter | 1 | 3.5 | 2.0 | 105 |
| | 5 | 2.5 | 1.0 | 150 |
| Root Quality | 1 | 3.5 | 2.5 | 84 |
| | 5 | 2.5 | 1.0 | 150 |
| HAZ | 1 | 2.5 | 1.0 | 150 |
| | 5 | 2.5 | 2.0 | 75 |

Table 12. Weld tests

| Weld # | Specimen | Parameter set |
|--------|----------|---------------|
| 1 | V11 | 1 |
| 2 | H21 | 1 |
| 3 | VH31 | 1 |
| 4 | HH41 | 1 |
| 5 | V12 | 2 |
| 6 | H22 | 2 |
| 7 | VH32 | 2 |
| 8 | HH42 | 2 |
| 9 | V13 | 3 |
| 10 | H23 | 3 |
| 11 | VH33 | 3 |
| 12 | HH43 | 3 |
| 13 | V14 | 4 |
| 14 | H24 | 4 |
| 15 | VH34 | 4 |
| 16 | HH44 | 4 |
| 17 | V15 | 5 |
| 18 | H25 | 5 |
| 19 | VH35 | 5 |
| 20 | HH45 | 5 |
| 21 | V16 | 6 |
| 22 | H26 | 6 |
| 23 | VH36 | 6 |
| 24 | HH46 | 6 |
| 25 | V17 | 7 |
| 26 | H27 | 7 |
| 27 | VH37 | 7 |
| 28 | HH47 | 7 |
| 29 | V18 | 8 |
| 30 | H28 | 8 |
| 31 | VH38 | 8 |
| 32 | HH48 | 8 |
| 33 | V19 | 9 |
| 34 | H29 | 9 |
| 35 | VH39 | 9 |
| 36 | HH49 | 9 |

APPENDIX II, 2

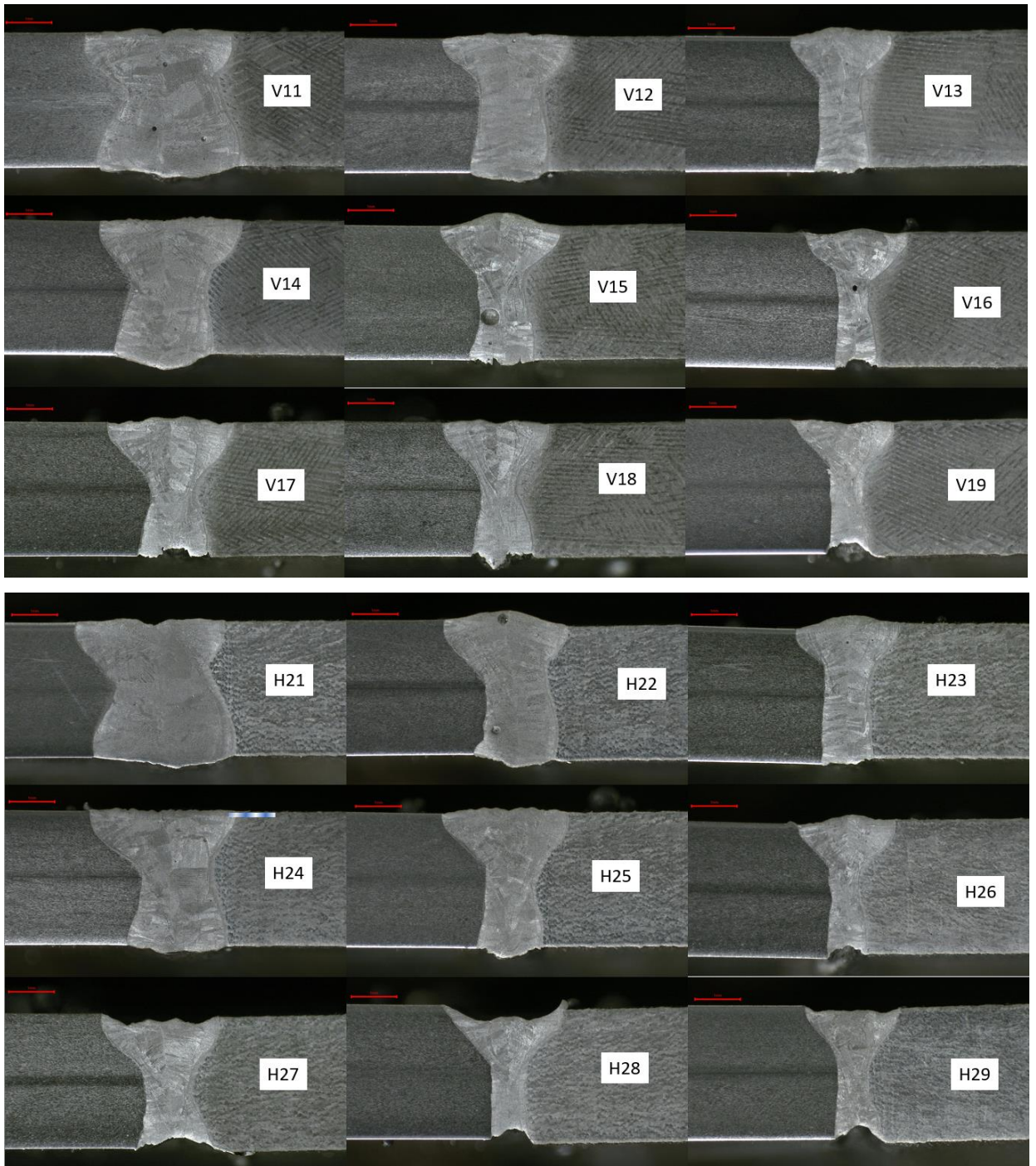
| 2.5 kW as constant power | | | | | | | | | | | | | | | |
|--------------------------|------------|-------|-------|----------|------------|-------|-------|----------|------------|-------|-------|----------|------------|-------|-------|
| Overall quality | | | | | | | | | | | | | | | |
| VB | | | | HB | | | | VBHT | | | | HBHT | | | |
| Specimen | Heat input | Speed | Grade | Specimen | Heat input | Speed | Grade | Specimen | Heat input | Speed | Grade | Specimen | Heat input | Speed | Grade |
| V11 | 150 | 1.0 | 4 | H21 | 150 | 1.0 | 3,75 | VH31 | 150 | 1.0 | 4 | HH41 | 150 | 1.0 | 3,75 |
| V12 | 100 | 1.5 | 4,25 | H22 | 100 | 1.5 | 4,25 | VH32 | 100 | 1.5 | 4 | HH42 | 100 | 1.5 | 4,25 |
| V13 | 75 | 2.0 | 4,75 | H23 | 75 | 2.0 | 4,75 | VH33 | 75 | 2.0 | 4 | HH43 | 75 | 2.0 | 4,5 |
| 3 | | | | | | | | | | | | | | | |
| Penetration | | | | | | | | | | | | | | | |
| VB | | | | HB | | | | VBHT | | | | HBHT | | | |
| Specimen | Heat input | Speed | Grade | Specimen | Heat input | Speed | Grade | Specimen | Heat input | Speed | Grade | Specimen | Heat input | Speed | Grade |
| V11 | 150 | 1.0 | 5 | H21 | 150 | 1.0 | 5 | VH31 | 150 | 1.0 | 5 | HH41 | 150 | 1.0 | 5 |
| V12 | 100 | 1.5 | 5 | H22 | 100 | 1.5 | 5 | VH32 | 100 | 1.5 | 5 | HH42 | 100 | 1.5 | 5 |
| V13 | 75 | 2.0 | 5 | H23 | 75 | 2.0 | 5 | VH33 | 75 | 2.0 | 5 | HH43 | 75 | 2.0 | 5 |
| Spatter | | | | | | | | | | | | | | | |
| VB | | | | HB | | | | VBHT | | | | HBHT | | | |
| Specimen | Heat input | Speed | Grade | Specimen | Heat input | Speed | Grade | Specimen | Heat input | Speed | Grade | Specimen | Heat input | Speed | Grade |
| V11 | 150 | 1.0 | 5 | H21 | 150 | 1.0 | 4 | VH31 | 150 | 1.0 | 5 | HH41 | 150 | 1.0 | 4 |
| V12 | 100 | 1.5 | 5 | H22 | 100 | 1.5 | 5 | VH32 | 100 | 1.5 | 4 | HH42 | 100 | 1.5 | 5 |
| V13 | 75 | 2.0 | 5 | H23 | 75 | 2.0 | 5 | VH33 | 75 | 2.0 | 3 | HH43 | 75 | 2.0 | 4 |
| Root quality | | | | | | | | | | | | | | | |
| VB | | | | HB | | | | VBHT | | | | HBHT | | | |
| Specimen | Heat input | Speed | Grade | Specimen | Heat input | Speed | Grade | Specimen | Heat input | Speed | Grade | Specimen | Heat input | Speed | Grade |
| V11 | 150 | 1.0 | 5 | H21 | 150 | 1.0 | 5 | VH31 | 150 | 1.0 | 5 | HH41 | 150 | 1.0 | 5 |
| V12 | 100 | 1.5 | 5 | H22 | 100 | 1.5 | 5 | VH32 | 100 | 1.5 | 5 | HH42 | 100 | 1.5 | 5 |
| V13 | 75 | 2.0 | 5 | H23 | 75 | 2.0 | 5 | VH33 | 75 | 2.0 | 4 | HH43 | 75 | 2.0 | 5 |
| HAZ | | | | | | | | | | | | | | | |
| VB | | | | HB | | | | VBHT | | | | HBHT | | | |
| Specimen | Heat input | Speed | Grade | Specimen | Heat input | Speed | Grade | Specimen | Heat input | Speed | Grade | Specimen | Heat input | Speed | Grade |
| V11 | 150 | 1.0 | 1 | H21 | 150 | 1.0 | 1 | VH31 | 150 | 1.0 | 1 | HH41 | 150 | 1.0 | 1 |
| V12 | 100 | 1.5 | 2 | H22 | 100 | 1.5 | 2 | VH32 | 100 | 1.5 | 2 | HH42 | 100 | 1.5 | 2 |
| V13 | 75 | 2.0 | 4 | H23 | 75 | 2.0 | 4 | VH33 | 75 | 2.0 | 4 | HH43 | 75 | 2.0 | 4 |

| 3.0 kW as constant power | | | | | | | | | | | | | | | |
|--------------------------|------------|-------|-------|----------|------------|-------|-------|----------|------------|-------|-------|----------|------------|-------|-------|
| Overall quality | | | | | | | | | | | | | | | |
| VB | | | | HB | | | | VBHT | | | | HBHT | | | |
| Specimen | Heat input | Speed | Grade | Specimen | Heat input | Speed | Grade | Specimen | Heat input | Speed | Grade | Specimen | Heat input | Speed | Grade |
| V14 | 120 | 1.5 | 4,5 | H24 | 120 | 1.5 | 4,25 | VH34 | 120 | 1.5 | 3,75 | HH44 | 120 | 1.5 | 4 |
| V15 | 90 | 2.0 | 4 | H25 | 90 | 2.0 | 4 | VH35 | 90 | 2.0 | 3,5 | HH45 | 90 | 2.0 | 3,5 |
| V16 | 72 | 2.5 | 3,75 | H26 | 72 | 2.5 | 3,5 | VH36 | 72 | 2.5 | 3,5 | HH46 | 72 | 2.5 | 3,75 |
| Penetration | | | | | | | | | | | | | | | |
| VB | | | | HB | | | | VBHT | | | | HBHT | | | |
| Specimen | Heat input | Speed | Grade | Specimen | Heat input | Speed | Grade | Specimen | Heat input | Speed | Grade | Specimen | Heat input | Speed | Grade |
| V14 | 120 | 1.5 | 5 | H24 | 120 | 1.5 | 5 | VH34 | 120 | 1.5 | 4 | HH44 | 120 | 1.5 | 5 |
| V15 | 90 | 2.0 | 5 | H25 | 90 | 2.0 | 5 | VH35 | 90 | 2.0 | 4 | HH45 | 90 | 2.0 | 4 |
| V16 | 72 | 2.5 | 4 | H26 | 72 | 2.5 | 4 | VH36 | 72 | 2.5 | 5 | HH46 | 72 | 2.5 | 5 |
| Spatter | | | | | | | | | | | | | | | |
| VB | | | | HB | | | | VBHT | | | | HBHT | | | |
| Specimen | Heat input | Speed | Grade | Specimen | Heat input | Speed | Grade | Specimen | Heat input | Speed | Grade | Specimen | Heat input | Speed | Grade |
| V14 | 120 | 1.5 | 5 | H24 | 120 | 1.5 | 4 | VH34 | 120 | 1.5 | 3 | HH44 | 120 | 1.5 | 3 |
| V15 | 90 | 2.0 | 3 | H25 | 90 | 2.0 | 3 | VH35 | 90 | 2.0 | 2 | HH45 | 90 | 2.0 | 2 |
| V16 | 72 | 2.5 | 3 | H26 | 72 | 2.5 | 3 | VH36 | 72 | 2.5 | 2 | HH46 | 72 | 2.5 | 2 |
| Root quality | | | | | | | | | | | | | | | |
| VB | | | | HB | | | | VBHT | | | | HBHT | | | |
| Specimen | Heat input | Speed | Grade | Specimen | Heat input | Speed | Grade | Specimen | Heat input | Speed | Grade | Specimen | Heat input | Speed | Grade |
| V14 | 120 | 1.5 | 5 | H24 | 120 | 1.5 | 5 | VH34 | 120 | 1.5 | 5 | HH44 | 120 | 1.5 | 5 |
| V15 | 90 | 2.0 | 4 | H25 | 90 | 2.0 | 4 | VH35 | 90 | 2.0 | 4 | HH45 | 90 | 2.0 | 4 |
| V16 | 72 | 2.5 | 3 | H26 | 72 | 2.5 | 2 | VH36 | 72 | 2.5 | 2 | HH46 | 72 | 2.5 | 3 |
| HAZ | | | | | | | | | | | | | | | |
| VB | | | | HB | | | | VBHT | | | | HBHT | | | |
| Specimen | Heat input | Speed | Grade | Specimen | Heat input | Speed | Grade | Specimen | Heat input | Speed | Grade | Specimen | Heat input | Speed | Grade |
| V14 | 120 | 1.5 | 3 | H24 | 120 | 1.5 | 3 | VH34 | 120 | 1.5 | 3 | HH44 | 120 | 1.5 | 3 |
| V15 | 90 | 2.0 | 4 | H25 | 90 | 2.0 | 4 | VH35 | 90 | 2.0 | 4 | HH45 | 90 | 2.0 | 4 |
| V16 | 72 | 2.5 | 5 | H26 | 72 | 2.5 | 5 | VH36 | 72 | 2.5 | 5 | HH46 | 72 | 2.5 | 5 |

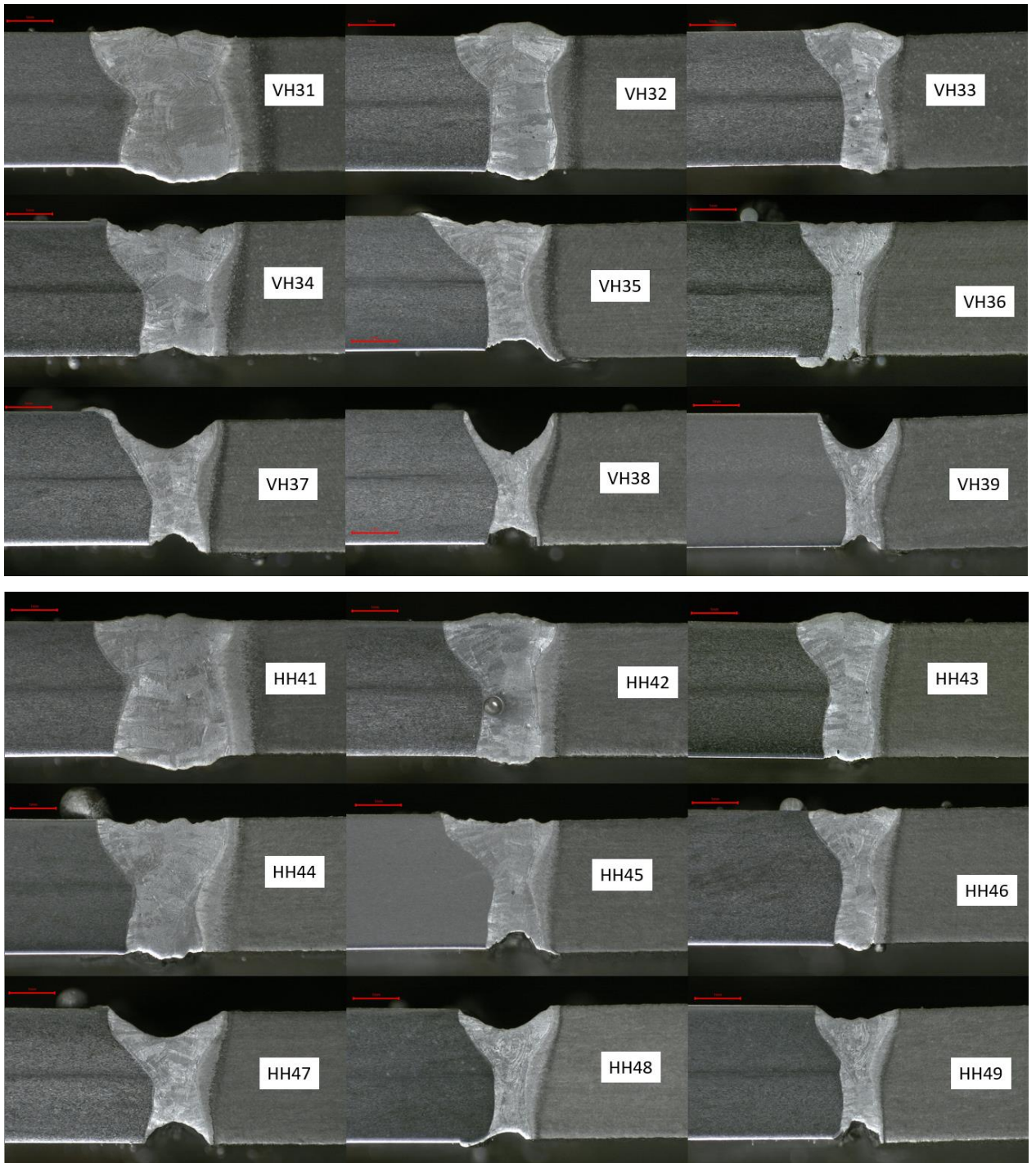
APPENDIX II, 3

| 3.5 kW as constant power | | | | | | | | | | | | | | | |
|--------------------------|------------|-------|-------|----------|------------|-------|-------|----------|------------|-------|-------|----------|------------|-------|-------|
| Overall quality | | | | | | | | | | | | | | | |
| VB | | | | HB | | | | VBHT | | | | HBHT | | | |
| Specimen | Heat input | Speed | Grade | Specimen | Heat input | Speed | Grade | Specimen | Heat input | Speed | Grade | Specimen | Heat input | Speed | Grade |
| V17 | 105 | 2.0 | 2,75 | H27 | 105 | 2.0 | 3 | VH37 | 105 | 2.0 | 2,5 | HH47 | 105 | 2.0 | 2,25 |
| V18 | 84 | 2.5 | 3,25 | H28 | 84 | 2.5 | 2,75 | VH38 | 84 | 2.5 | 3 | HH48 | 84 | 2.5 | 3 |
| V19 | 70 | 3.0 | 3,25 | H29 | 70 | 3.0 | 3,5 | VH39 | 70 | 3.0 | 3,5 | HH49 | 70 | 3.0 | 3,25 |
| Penetration | | | | | | | | | | | | | | | |
| VB | | | | HB | | | | VBHT | | | | HBHT | | | |
| Specimen | Heat input | Speed | Grade | Specimen | Heat input | Speed | Grade | Specimen | Heat input | Speed | Grade | Specimen | Heat input | Speed | Grade |
| V17 | 105 | 2.0 | 4 | H27 | 105 | 1.5 | 4 | VH37 | 105 | 2.0 | 2 | HH47 | 105 | 2.0 | 2 |
| V18 | 84 | 2.5 | 5 | H28 | 84 | 2.0 | 3 | VH38 | 84 | 2.5 | 2 | HH48 | 84 | 2.5 | 3 |
| V19 | 70 | 3.0 | 4 | H29 | 70 | 2.5 | 4 | VH39 | 70 | 3.0 | 2 | HH49 | 70 | 3.0 | 3 |
| Spatter | | | | | | | | | | | | | | | |
| VB | | | | HB | | | | VBHT | | | | HBHT | | | |
| Specimen | Heat input | Speed | Grade | Specimen | Heat input | Speed | Grade | Specimen | Heat input | Speed | Grade | Specimen | Heat input | Speed | Grade |
| V17 | 105 | 2.0 | 2 | H27 | 105 | 1.5 | 2 | VH37 | 105 | 2.0 | 2 | HH47 | 105 | 2.0 | 1 |
| V18 | 84 | 2.5 | 2 | H28 | 84 | 2.0 | 2 | VH38 | 84 | 2.5 | 3 | HH48 | 84 | 2.5 | 3 |
| V19 | 70 | 3.0 | 3 | H29 | 70 | 2.5 | 3 | VH39 | 70 | 3.0 | 4 | HH49 | 70 | 3.0 | 3 |
| Root quality | | | | | | | | | | | | | | | |
| VB | | | | HB | | | | VBHT | | | | HBHT | | | |
| Specimen | Heat input | Speed | Grade | Specimen | Heat input | Speed | Grade | Specimen | Heat input | Speed | Grade | Specimen | Heat input | Speed | Grade |
| V17 | 105 | 2.0 | 2 | H27 | 105 | 1.5 | 3 | VH37 | 105 | 2.0 | 3 | HH47 | 105 | 2.0 | 3 |
| V18 | 84 | 2.5 | 2 | H28 | 84 | 2.0 | 2 | VH38 | 84 | 2.5 | 3 | HH48 | 84 | 2.5 | 2 |
| V19 | 70 | 3.0 | 1 | H29 | 70 | 2.5 | 2 | VH39 | 70 | 3.0 | 3 | HH49 | 70 | 3.0 | 2 |
| HAZ | | | | | | | | | | | | | | | |
| VB | | | | HB | | | | VBHT | | | | HBHT | | | |
| Specimen | Heat input | Speed | Grade | Specimen | Heat input | Speed | Grade | Specimen | Heat input | Speed | Grade | Specimen | Heat input | Speed | Grade |
| V17 | 105 | 2.0 | 3 | H27 | 105 | 1.5 | 3 | VH37 | 105 | 2.0 | 3 | HH47 | 105 | 2.0 | 3 |
| V18 | 84 | 2.5 | 4 | H28 | 84 | 2.0 | 4 | VH38 | 84 | 2.5 | 4 | HH48 | 84 | 2.5 | 4 |
| V19 | 70 | 3.0 | 5 | H29 | 70 | 2.5 | 5 | VH39 | 70 | 3.0 | 5 | HH49 | 70 | 3.0 | 5 |

APPENDIX III, 1



APPENDIX III, 2



APPENDIX III, 3



APPENDIX III, 4

